Effects of pre-stress state and rupture velocity on dynamic fault branching

Nobuki Kame, James R. Rice and Renata Dmowska

Department of Earth and Planetary Sciences and Division of Engineering and Applied Sciences, Harvard University, Cambridge, Massachusetts

Abstract. We consider a mode II rupture which propagates along a planar main fault and encounters an intersection with a branching fault. Using an elastodynamic boundary integral equation formulation, allowing the failure path to be dynamically self-chosen, we study the following questions: Does the rupture initiate along the branch? Does it continue? Is the extensional or compressional side most favored for branching? Does rupture continue on the main fault too? Failure is described by a slip-weakening law for which the strength at any amount of slip is proportional to normal stress.

Our results show that dynamic stresses around the rupture tip, which increase with rupture velocity at locations off the main fault plane relative to those on it, could initiate rupture on a branching fault. As suggested by prior work, whether branched rupture can be continued to a larger scale depends on principal stress directions in the pre-stress state and on rupture velocity. The most favored side for branching rupture switches from the extensional to the compressional side as we consider progressively shallower angles of the direction of maximum compressive pre-stress with the main fault. Simultaneous rupturing on both faults can be activated when the branching angle is wide, but is usually difficult for a narrow branching angle due to strong stress interactions between faults. However, it can be activated then too by enhanced dynamic stressing when the rupture velocity is very near the Rayleigh velocity. Natural examples seem consistent with the simulations we present.

1. Introduction

The rupture zones of major earthquakes often involve geometric complexities including fault bends, branches and stepovers. Such non-planar fault structures have been suggested to affect the dynamic rupture process including nucleation, propagation and termination [*King and Nabelek*, 1985; *Sibson*, 1985]. In this paper, we focus on branched faults. Several earthquakes have occurred along preexisting fault structures that include branching faults [*King*, 1986]. The 1979 Imperial Valley and the 1992 Landers earthquake are examples [*Archuleta*, 1984; *Sowers et al.*, 1994]. What path is dynamically self-chosen in a pre-existing geometrically complex fault system, with branches or step-overs, is very important for seismic risk estimates.

Theoretical stress analysis for mode II rupture running on a planar fault suggests that the propensity of rupture path to bend onto a potential branch path is controlled by rupture velocity v_r and the preexisting stress state [*Poliakov et al.*, 2002]. In describing rupture by a slip-weakening model, deviatoric stresses in the vicinity of a rapidly propagating rupture front are found to be much higher in the border region, to the side of the fault plane than directly ahead, when rupture velocity v_r becomes close to the limiting velocity, which is the Rayleigh wave velocity c_R for mode II. The pattern of predicted Coulomb failure on secondary faults, within a damaged zone bordering the main fault, is strongly dependent on the angle Ψ between the planar fault and the direction of maximum compression S_{max} in a pre-stress field. High S_{max} angles Ψ lead to more extensive activation of secondary faulting on the extensional side, whereas low angles give comparable activation on both sides. In both cases, secondary failure off the planar fault is predicted to increase markedly as the limiting velocity is approached (Figure 1). However, the theoretical solutions just discussed are limited to the cases where ruptures remain on a plane and no further alterations of the stress field due to the excitation of secondary ruptures has been considered, in the interest of mathematical simplicity. Accordingly, what path is dynamically self-chosen on a branched fault system still remains unknown. The dynamics, including nucleation of secondary ruptures, must be investigated with numerical methods.

Recent progress in the boundary integral equation method (BIEM) has enabled simulation of spontaneous rupture with a complex fault geometry. *Kame and Yamashita* [1999a, 1999b, 2002] have investigated dynamic branching in their self-chosen crack path modeling. They base the choice of the orientation of each new increment of crack path on the maximum shear stress along radial directions very near the crack tip, explicitly including the high-speed distortion of the stress field. They successfully showed that a crack bifurcates at the high-speed propagation stage due to localization of wave stresses around the crack tip and then the growth, after following the locally optimal path, is finally arrested, after branching, by the larger scale pre-stress state. However, it remains an open issue of how to properly include effects of normal stress in that description. In addition, the nature of their crack-tip-focused procedure does not allow

Effects of prestress state and rupture velocity on dynamic fault branching

Nobuki Kame,[1] James R. Rice, and Renata Dmowska

Department of Earth and Planetary Sciences and Division of Engineering and Applied Sciences, Harvard University, Cambridge, Massachusetts, USA

[1]   We consider a mode II rupture which propagates along a planar main fault and encounters an intersection with a branching fault. Using an elastodynamic boundary integral equation formulation, allowing the failure path to be dynamically self-chosen, we study the following questions: Does the rupture initiate along the branch? Does it continue? Is the extensional or compressional side most favored for branching? Does rupture continue on the main fault too? Failure is described by a slip-weakening law for which the strength at any amount of slip is proportional to normal stress. Our results show that dynamic stresses around the rupture tip, which increase with rupture velocity at locations off the main fault plane relative to those on it, could initiate rupture on a branching fault. As suggested by prior work, whether branched rupture can be continued to a larger scale depends on principal stress directions in the prestress state and on rupture velocity. The most favored side for branching rupture switches from the extensional to the compressional side as we consider progressively shallower angles of the direction of maximum compressive prestress with the main fault. Simultaneous rupturing on both faults can be activated when the branching angle is wide but is usually difficult for a narrow branching angle due to strong stress interactions between faults. However, it can be also be activated by enhanced dynamic stressing when the rupture velocity is very near the Rayleigh velocity. Natural examples seem consistent with the simulations that we present.   *INDEX TERMS:* 7209 Seismology: Earthquake dynamics and mechanics; 7223 Seismology: Seismic hazard assessment and prediction; 7260 Seismology: Theory and modeling; 8010 Structural Geology: Fractures and faults; *KEYWORDS:* branching, fault, rupture propagation, boundary integral equation method (BIEM), fracture

1. Introduction

[2]   The rupture zones of major earthquakes often involve geometric complexities including fault bends, branches and step overs. Such nonplanar fault structures have been suggested to affect the dynamic rupture process including nucleation, propagation and termination [*King and Nabelek*, 1985; *Sibson*, 1985]. In this paper, we focus on branched faults. Several earthquakes have occurred along preexisting fault structures that include branching faults [*King*, 1986]. The 1979 Imperial Valley and the 1992 Landers earthquake are examples [*Archuleta*, 1984; *Sowers et al.*, 1994]. What path is dynamically self-chosen in a preexisting geometrically complex fault system, with branches or step overs, is very important for seismic risk estimates.

[3]   Theoretical stress analysis for mode II rupture running on a planar fault suggests that the propensity of rupture path to bend onto a potential branch path is controlled by rupture velocity v_r and the preexisting stress state [*Poliakov et al.*, 2002]. In describing rupture by a slip-weakening model, deviatoric stresses in the vicinity of a rapidly propagating rupture front are found to be much higher in the border region, to the side of the fault plane than directly ahead, when rupture velocity v_r becomes close to the limiting velocity, which is the Rayleigh wave velocity c_R for mode II. The pattern of predicted Coulomb failure on secondary faults, within a damaged zone bordering the main fault, is strongly dependent on the angle Ψ between the planar fault and the direction of maximum compression S_{max} in a prestress field. High S_{max} angles Ψ lead to more extensive activation of secondary faulting on the extensional side, whereas low angles give comparable activation on both sides. In both cases, secondary failure off the planar fault is predicted to increase markedly as the limiting velocity is approached (Figure 1). However, the theoretical solutions just discussed are limited to the cases where ruptures remain on a plane and no further alterations of the stress field due to

---
[1]Now at Department of Earth and Planetary Sciences, Kyushu University, Fukuoka, Japan.
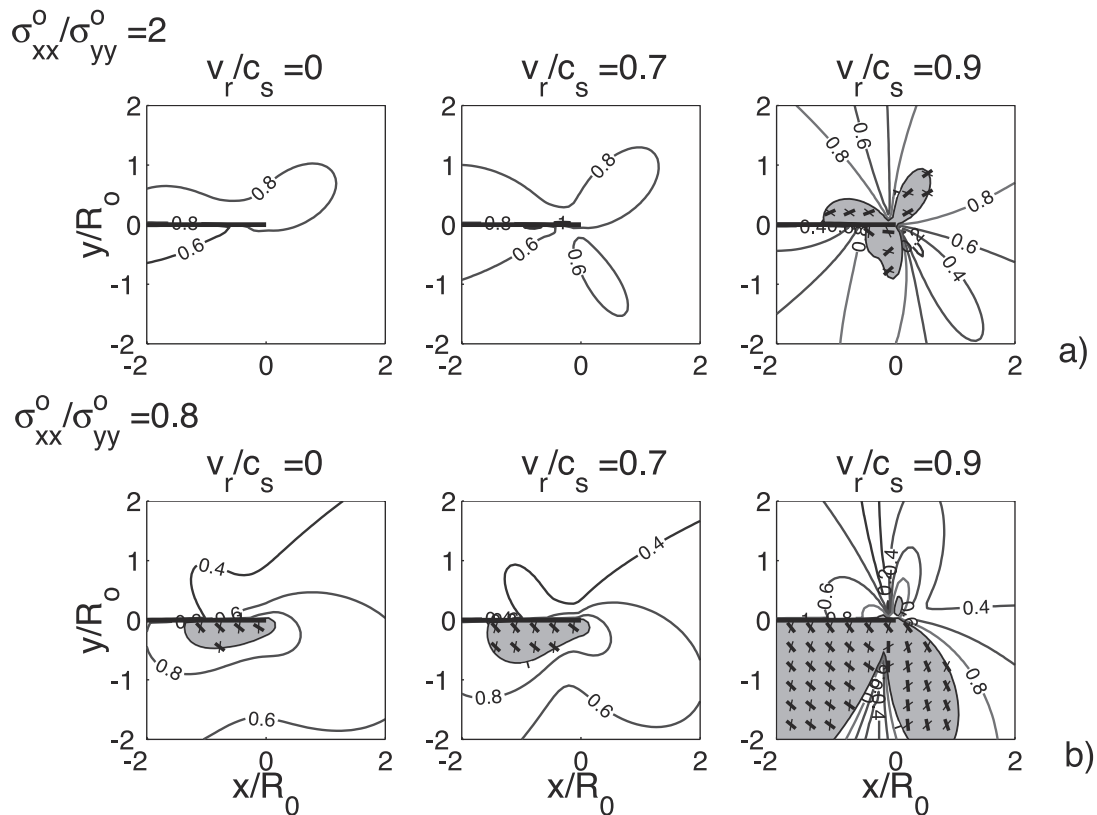
Figure 1. Illustrations of dynamic elastic stress fields associated with slip-weakening rupture on a planar fault for two prestress ratios and different rupture velocities v_r. This is Figure 11 of *Poliakov et al.* [2002]. (a) When $(-\sigma_{yy}^0) < (-\sigma_{xx}^0)$. Here $(-\sigma_{xx}^0)/(-\sigma_{yy}^0) = 2.0$ corresponds to low inclination of S_{max} with respect to the fault plane. (b) When $(-\sigma_{yy}^0) > (-\sigma_{xx}^0)$. $(-\sigma_{xx}^0)/(-\sigma_{yy}^0) = 0.8$ corresponds to high inclination of S_{max}. The shaded regions show where the maximum local shear stress τ_{max} exceeds to Coulomb strength $\tau_{Coulomb}$ based on the local normal stresses, and the expected Mohr-Coulomb rupture directions are shown. Contour lines of $\tau_{max}/\tau_{Coulomb}$ are shown where it is less than unity, outside the shaded zone.

the excitation of secondary ruptures has been considered, in the interest of mathematical simplicity. Accordingly, what path is dynamically self-chosen on a branched fault system still remains unknown. The dynamics, including nucleation of secondary ruptures, must be investigated with numerical methods.

[4] Recent progress in the boundary integral equation method (BIEM) has enabled simulation of spontaneous rupture with a complex fault geometry. *Kame and Yamashita* [1999a, 1999b, also Dynamic branching, arresting of rupture and seismic wave radiation in self-chosen crack path modeling, submitted to *Geophysical Journal International*, 2002] have investigated dynamic branching in their self-chosen crack path modeling. They base the choice of the orientation of each new increment of crack path on the maximum shear stress along radial directions very near the crack tip, explicitly including the high-speed distortion of the stress field. They successfully showed that a crack bifurcates at the high-speed propagation stage due to localization of wave stresses around the crack tip and then the growth, after following the locally optimal path, is finally arrested, after branching, by the larger scale prestress state. However, it remains an open issue of how to properly include effects of normal stress in

that description. In addition, the nature of their crack-tip-focused procedure does not allow for the possibility of renucleation of rupture on the main fault plane after branching, which is a critical feature for the overall rupture dynamics. *Aochi et al.* [2000a, 2000b] simulated a spontaneous rupture process on a curved fault and a branched fault in three dimensions. *Aochi and Fukuyama* [2002] applied such an approach to understanding the 1992 Landers earthquake and discussed the importance of the prestress orientation on rupture selectivity on a branched fault. That work also based the failure criterion on only the shear stress at the rupture tip, although very recently *Aochi et al.* [2002] have extended this approach to include the effects of normal stresses as well. The effect of rupture velocity v_r has remained unexamined in their simulations partly because they could not take a small enough spatial grid spacing in 3-D simulations to resolve off-plane stressing at the high-speed propagation stage or to keep the speed subshear.

[5] Our aim here is to investigate by numerical elastodynamics the effects of prestress state and rupture velocity on dynamic branching, thus examining the validity of and quantifying the somewhat qualitative prediction of their effects by *Poliakov et al.* [2002] based on stress fields of
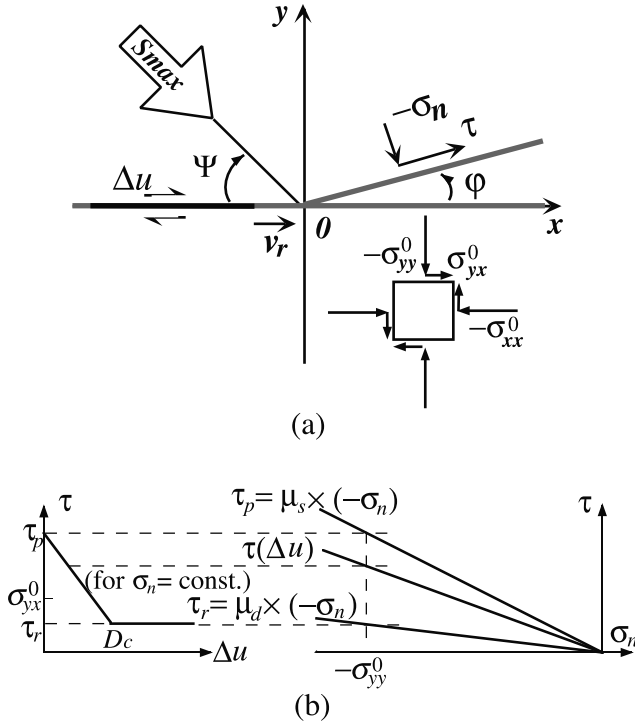
Figure 2. Model configuration and assumed slip-weakening Coulomb friction law. (a) Configuration of a preexisting branched fault system and prestress state. Gray lines indicate potential rupture surface and black line indicates propagating rupture. τ and $-\sigma_n$ represent shear stress and compressive normal stress on fault surface. (b) Slip-weakening Coulomb friction law. The peak and residual strength (τ_p, τ_r), and strength (τ) at any particular amount of slip (Δu), is proportional to normal stress ($-\sigma_n$).

nonbranched ruptures. For that purpose, we consider a mode II rupture which propagates along a planar main fault and encounters an intersection with a branching fault that makes an angle with the main fault. We use the elastodynamic boundary integral equation method proposed by *Kame and Yamashita* [1999b] to allow simulations of rupture in which the failure path is dynamically self-chosen. We describe failure in the modeling by a slip-weakening Coulomb friction law for which the peak and residual strength, and strength at any particular amount of slip, is proportional to normal stress. We will see how rupture dynamically chooses its path on a branched fault under the effects of the prestress state and the rupture velocity.

2. Model

2.1. Configuration of Branched Fault and Prestress State

[6] We consider a mode II rupture which propagates along a planar fault and encounters an intersection with a branching fault that makes an angle φ with the main fault (Figure 2a). The fault system is embedded in an unbounded homogeneous isotropic elastic medium. We use a Cartesian coordinates (x, y) and configure the main fault plane on the x axis and the intersection point at the origin. We assume that the fault surface is closed everywhere, that is, there is tangential

slip only and no opening (purely mode II). Prestress is presumed to act on the medium as $(-\sigma_{xx}^0) > 0$, $(\sigma_{yx}^0) > 0$ and $(-\sigma_{yy}^0) > 0$ (we take tension as positive), and the direction of maximum precompression S_{max} makes an angle Ψ with the main fault plane. Angles $\Psi < 45°$ result when the ratio $(-\sigma_{xx}^0)/(-\sigma_{yy}^0)$ of fault-parallel to fault-normal precompression, is greater than unity. Note that by the pure antisymmetry relative to the x axis, as long as rupture propagates along the main plane only, the fault normal compression $(-\sigma_{yy})$ there will not alter from the precompression $(-\sigma_{yy}^0)$. Such will not be the case for either the main or branch plane when rupture extends along the branch.

2.2. Slip-Weakening Coulomb Friction Law

[7] Failure in the modeling is described by a slip-weakening friction law originally proposed by *Ida* [1972] and *Palmer and Rice* [1973]. The fault strength τ, once reaching the peak strength τ_p, decreases linearly to the residual strength τ_r with ongoing fault slip Δu. In addition, we introduce Coulomb friction law into the slip-weakening law, which describes τ as a linear function of normal stress $(-\sigma_n)$ and has been widely used to study friction on faults. Under the slip-weakening Coulomb friction law, the fault strength τ at any particular amount of slip is proportional to normal stress $(-\sigma_n)$ as (see Figure 2b),

$$\tau = \tau_r + (\tau_p - \tau_r)(1 - \Delta u/D_c)H(1 - \Delta u/D_c), \quad (1)$$

where

$$\tau_p = \mu_s \times (-\sigma_n), \qquad \tau_r = \mu_d \times (-\sigma_n). \quad (2)$$

Here μ_s, μ_d, $H(\cdot)$ and D_c are static friction coefficient, dynamic friction coefficient, Heaviside function and critical slip displacement respectively.

[8] The minimum nucleation size L_c determined by the energy balance is represented in terms of the slip-weakening parameters (when the Poisson ratio is 0.25, as here) by

$$L_c = \frac{16}{3\pi} \frac{\mu G}{\left(\sigma_{yx}^0 - \tau_r\right)^2} = \frac{64}{9\pi^2} \left(\frac{\tau_p - \tau_r}{\sigma_{yx}^0 - \tau_r}\right)^2 R_0, \quad (3)$$

where μ is the shear modulus and G is the fracture energy of the medium. Here $R_0 = (3\pi/4)[\mu G/(\tau_p - \tau_r)^2]$ is the expression of *Palmer and Rice* [1973] and *Rice* [1980] for the length of the static slip-weakening zone; that expression for R_0 becomes exact for their particular slip-weakening law, as does equation (3) also, if the parameters chosen make $L_c \gg R_0$.

[9] In this paper, rupture is allowed only on the preexisting fault structure, where these frictional properties are assumed to be uniform over the whole fault system and the coefficients are taken as $\mu_s = 0.60$ and $\mu_d = 0.12$. In this first presentation we neglect fluid saturation and stress-induced pore pressure changes, briefly discussed by *Poliakov et al.* [2002]; in a certain limiting case [*Cocco and Rice*, 2002] their effect can be modeled by choice of an appropriately reduced value for μ_s.

2.3. Boundary Integral Equation Method

[10] Following *Kame and Yamashita* [1999b], the incremental shear stress $\Delta\tau$ due to the slip on a fault is evaluated

only in terms of the past slip rate history over the fault. Applying a discretization where a constant slip velocity (V) is assumed within each spatial element (of size Δs) and during each time step t to $t + \Delta t$, we can concisely write the BIE for $\Delta \tau$, at the center of cell l at the end of time step n, in the following symbolic notation, when $\Delta t \leq \Delta s/(2c_d)$:

$$\Delta \tau^{ln} = K_\tau^{00:00} V^{ln} + \sum_{k=0}^{n-1} \sum_i K_\tau^{ln:ik} V^{ik}. \qquad (4)$$

Here l and i represent the discretized position on the fault and n and k represent the discretized time step. c_d is the dilational (p wave) speed. The first term on the right hand side, $K_\tau^{00:00} = -\mu/2c_s$, is the radiation damping term [*Cochard and Madariaga*, 1994] that represents the instantaneous contribution of the current slip velocity to the shear stress at the same position (μ is shear rigidity, c_s is shear wave speed). The second term contains the contribution of the past slip rate history; $K_\tau^{ln:ik}$ indicates the stress at the center of cell l, at the end of time step n, due to imposing a unit slip rate within cell i during time step k. The sum on i must be carried out over all cells which are fully or partly within the p wave cone extending backward in time from the center of cell l at the end of time step n. The incremental normal stress $\Delta \sigma_n$ has a similar symbolic form except that its instantaneous term is zero as long as we consider no opening on faults. This property simplifies the solving of equation (4) for the determination of $\Delta \tau^{ln}$ and V^{ln} under the normal-stress-dependent boundary condition (equations (1) and (2)). Note that the total stress, a sum of the incremental stress and the prestress, is considered in meeting the constitutive relation and note too that the incremental normal stress is not zero when we consider interacting elements with different orientation.

2.4. Dependence on Parameters

[11] Our aim here is to investigate the effects of prestress state and rupture velocity on the dynamically self-chosen path on a branched fault system. Before simulating dynamic rupture, we briefly review the possibility of rupture propagation onto a branching fault based on the more qualitative theoretical analysis by *Poliakov et al.* [2002]. Then we additionally mention the effect of another factor, the branching angle, that does not appear in the stress analysis of a planar fault.

2.4.1. Dependence on Prestress State

[12] The prestress state can be crucial for continuation of rupture, once begun, along a branch fault. We assume that the rupture is right-lateral. Consider a volume under maximum and minimum compressive principal stresses, S_{max} and S_{min}, like in Figure 3. Relative to the principal directions, there are two quadrants of fault orientation for which right-lateral slip is encouraged by the shear stress, as marked in Figure 3. There are two distinct limiting regimes, depending on the ratio of the fault-parallel precompression, $(-\sigma_{xx}^0)$, to the fault-normal precompression, $(-\sigma_{yy}^0)$. The fault-normal precompression is greater in Figure 3a, and the fault-parallel precompression is greater in Figure 3b. When $\sigma_{xx}^0 = \sigma_{yy}^0$, the S_{max} direction of the prestress makes an angle $\Psi = 45$ with the main fault plane. However, when $(-\sigma_{yy}^0) > (-\sigma_{xx}^0)$, like in Figure 3a, S_{max} makes an angle Ψ greater than 45°, whereas when the fault-parallel precompression is dominant, so that $(-\sigma_{yy}^0) < (-\sigma_{xx}^0)$ like in
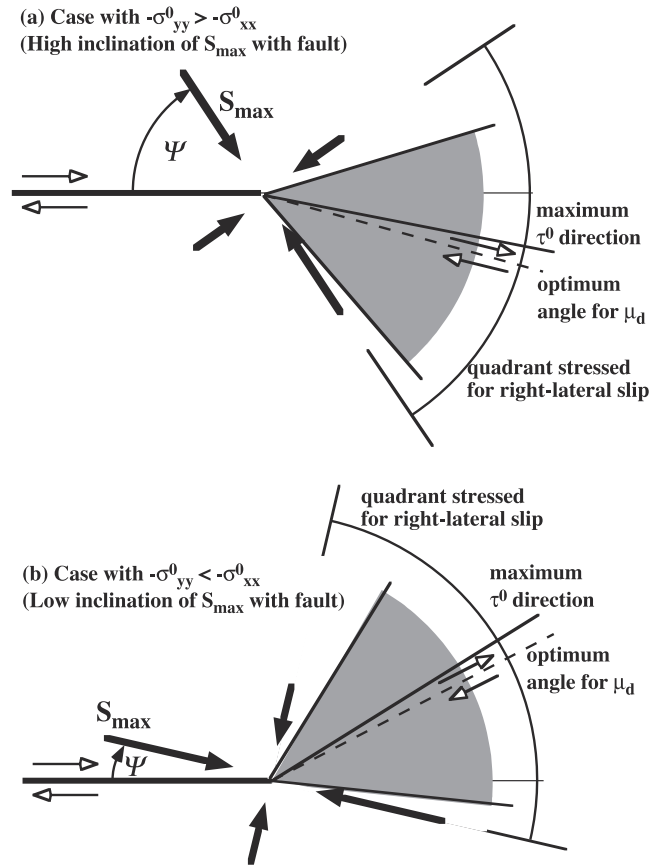

Figure 3. Qualitative prediction of the directions over which the larger scale prestress states favor right-lateral shear along bend paths. (a) Fault-normal precompression is dominant, $(-\sigma_{yy}^0) > (-\sigma_{xx}^0)$: Ψ is greater than 45°, allowing rupture to continue along bend paths primarily to the extensional side. (b) Fault-parallel precompression is dominant, $(-\sigma_{yy}^0) < (-\sigma_{xx}^0)$: S_{max} makes an angle Ψ smaller than 45° with the fault plane, allowing rupture to continue along bend paths primarily to the compressional side. The gray zones indicate the angle range where the initial shear stress τ^0 is larger than the frictional resistance $\mu_d(-\sigma_n^0)$.

Figure 3b, S_{max} makes an angle Ψ smaller than 45° with the main fault. Those differences mean that different angular zones experience right-lateral shear stress, and that the direction of maximum shear prestress τ^0 switches sides of the fault, depending on whether the fault-normal precompression is smaller or larger than the fault-parallel component. The prestress state should control whether propagation can be continued far from the branching point, once rupture is initiated on the branch. Figure 3a predicts that when the fault normal precompression is large compared to the fault parallel, so that Ψ is large, the stress state could allow rupture to continue along bent paths primarily to the extensional side, but would inhibit continuation on the compressional side. When the fault-parallel precompression is instead large (Figure 3b), so that Ψ is small, the stress state could encourage ruptures to continue on bent paths to the compressional side and inhibit the extensional (even though the compressional side is less favored for nucleation along a bent path [*Poliakov et al.*, 2002]).
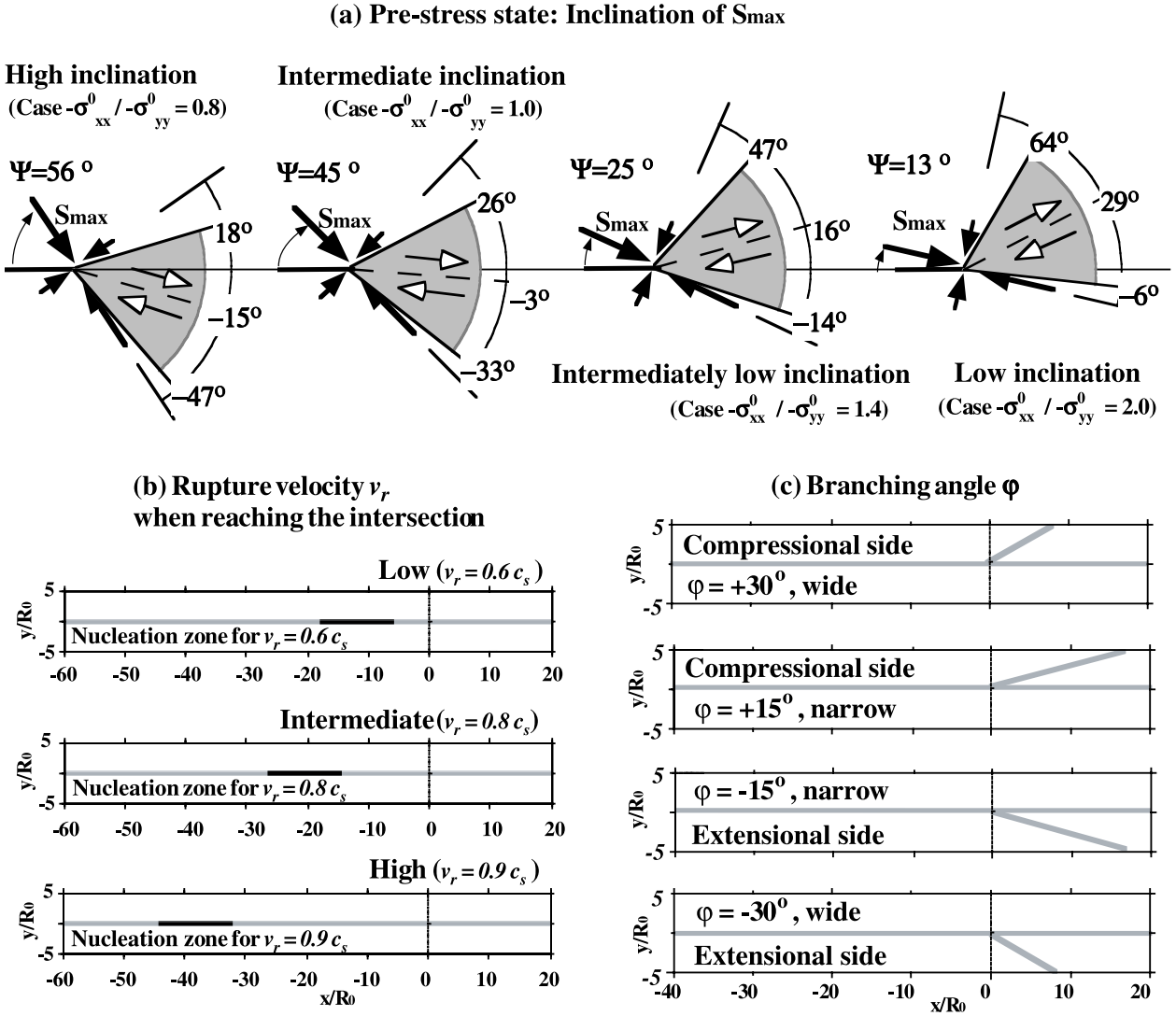
(a) Pre-stress state: Inclination of S_{max}

(b) Rupture velocity v_r when reaching the intersection

(c) Branching angle φ

Figure 4. Three parameters specified in the simulations. (a) Prestress state: Ψ is maximum compression angle. The gray zones indicate angle ranges where right-lateral slip is encouraged against dynamic Coulomb friction for each prestress state. The dotted line indicates the most favored plane for right-lateral slip. Two angles for the gray zone boundary and the most favored angle are indicated for reference. (b) Rupture velocity v_r: v_r entering the intersection point $(x, y) = (0, 0)$ is controlled by the position of the nucleation zone. (c) Branching angle φ: Four types of preexisting branched fault system are considered.

[13] In either case, the angular range encouraged for right-lateral rupture is narrowed when we consider Coulomb friction on faults. The range where the shear prestress level τ^0 exceeds the dynamic friction level $\mu_d \times (-\sigma_n^0)$ in the prestress state is shaded in Figure 3. The difference $\tau^0 - \tau_r$ is usually denoted as the stress drop $\Delta\sigma$ (τ_r coincides with $\mu_d \times (-\sigma_n^0)$). As is well known from the Mohr stress circle, the most favored angle inclines by the angle $-1/2 \times \tan^{-1}\mu_d$ from the maximum τ_0 direction, as shown in our figures for $\mu_d = 0.12$, and the stress drop $\Delta\sigma$ takes its maximum at that optimum angle. In this paper we scale all stresses with the fault-normal prestress and fix the shear prestress as $(\sigma_{yx}^0)/(-\sigma_{yy}^0) = 0.24$. Then we specify for consideration four different fault-parallel prestress states $(-\sigma_{xx}^0)/(-\sigma_{yy}^0) = 0.8, 1.0, 1.4$ and 2.0. The corresponding S_{max} angles Ψ are $56°, 45°, 25°$ and $13°$ and denoted as

high, intermediate, intermediately low and low inclinations, respectively (see Figure 4a).

2.4.2. Dependence on Rupture Velocity

[14] A first perspective is provided by the stress field of the singular elastic crack model. *Kame and Yamashita* [1999a, 1999b] and *Poliakov et al.* [2002] plot the angular variation of the singular terms in the stress field and show that at $v_r \approx 0.8c_s$ the singular shear stress term along potential branches at $\varphi \neq 0$ ahead of the rupture tip is comparable to that on the main fault at $\varphi = 0$. At higher speeds, v_r approaching $c_R \approx 0.92c_s$ (for $c_d = \sqrt{3}c_s$ as we assume here), the branched orientations become very much more preferred. When normal stress is considered also, to evaluate a Coulomb measure of shear stress along potential branch orientations [*Poliakov et al.*, 2002], it is found that the branches to the extensional side are always more highly stressed than to the compres-

sional, but that at high enough v_r potential branches to both sides are subjected to higher Coulomb stress than is the main fault. Theoretical understanding of unsteady crack dynamics based on the singular model [*Freund*, 1990; *Broberg*, 1999] suggests that mode II ruptures which remain on a plane will always be driven toward speeds very close to c_R if they expand without diminution of their seismic stress drop. This perspective suggests that ruptures should usually accelerate toward the speed range for which stresses off the main fault plane are higher than those along it. Thus the initiation of failure along branch intersections with the main fault should be ubiquitous. Nevertheless, it is at least partly the larger scale stress field which, as just discussed, may control whether rupture, once initiated, can continue far along a branch, and unsuccessful branching attempts are expected to locally diminish the rupture speed along the main fault.

[15] The influence of rupture velocity in combination with prestress state was also investigated in a nonsingular slip-weakening representation by *Poliakov et al.* [2002] to characterize elastically predicted stress off the main fault plane in mode II. To simplify and minimize the number of parameters, they followed *Rice* [1979] in developing an asymptotic solution in which the slip-weakening zone size R is assumed to be very small compared to overall slipping region dimensions, and chose the special shear strength vs. slip relation, which he showed to exist, that causes the shear stress to vary linearly from peak strength τ_p to residual strength τ_r with spatial position x within the slip-weakening zone, no matter what is v_r. For any given slip-weakening law, R is largest at $v_r = 0^+$ and that size, denoted R_0, was chosen to normalize distance. We make the same choice in this paper. R/R_0 is a function of v_r and diminishes to 0 as $v_r \rightarrow c_R$. A representative result of *Poliakov et al.* [2002] is shown in Figure 1 for $\tau_r/\tau_p = 0.2$. Isolines of $\tau_{max}/\tau_{Coulomb}$ demonstrate that the stress level and size of the activated zone grow as rupture velocity increases. At $v_r/c_s \approx 0.9$ the size of the activated zone becomes comparable to the size of the low-velocity slip-weakening zone R_0 or can exceed it, like in the example in Figure 1b for which the maximum dimension of the secondary faulting zone on the extensional side is around $5R_0$.

[16] A striking feature in Figure 1 is that the shape of the activated zone also crucially depends on $(-\sigma_{xx}^0)/(-\sigma_{yy}^0)$. In their discussion of what we show here as Figure 3, the qualitative influence of the initial state stress ratio on the expected fracture pattern was already suggested. When $(-\sigma_{yy}^0) < (-\sigma_{xx}^0)$ like Figure 1a, secondary faulting consistent with branching was predicted to be encouraged on the compressional side too, and when $(-\sigma_{yy}^0) > (-\sigma_{xx}^0)$ like Figure 1b, on the extensional side. Here we can be more quantitative. The very small angle Ψ of the principal stress associated with Figure 1a allows equal activation of secondary faulting on both sides of the rupture. Somewhat larger Ψ values, and especially values of $\Psi > 45°$ like in Figure 1b, strongly favor secondary failure on the extensional side.

[17] In the numerical modeling reported here we investigate the effect of rupture velocity v_r when the rupture front just reaches the branching junction for the three values v_r/c_s = 0.6, 0.8 and 0.9, which we denote as low, intermediate and high rupture velocity. We start spontaneous rupture from the nucleation zone, and the rupture velocity increases monotonically with its growth. In order to control v_r at the

intersection point $(x, y) = (0, 0)$, we change the position of the initial nucleation zone, where a slip distribution just loses its static equilibrium (Figure 4b).

2.4.3. Dependence on Branching Angle

[18] The branching angle φ is another factor that also plays a critical role in the dynamically self-chosen rupture path on a branched fault, due to stress interaction between faults. That interaction was not considered explicitly in theoretical stress analyses of planar fault to investigate dynamic branching [*Poliakov et al.*, 2002]. The qualitative effect is very simple: It will be more difficult to propagate rupture simultaneously on both faults for a narrower angle. That is because once rupture begins to propagate on one side of the faults, stress around the rupture is released and it no longer encourages rupture on the other side. This is called the "stress shadow effect" [e.g., *Yamashita and Umeda*, 1994]. For a wider angle, we can expect a weaker interaction and rupture will propagate on each fault less dependently on the other. At the same time, the orientation of the branching fault itself is also important because the stress field from the main fault will be resolved differently onto branches with different orientations (see Figure 1). *Aochi et al.* [2000b] clearly showed the effect of interaction on branching rupture in their simulation. Here, we specify four cases for branching angle, $\varphi = \pm15°$, narrow, and $\pm30°$, wide. Branching angles $\varphi = -15°$, $-30°$ mean that the branch fault is on the extensional side and $\varphi = +15°$, $+30°$ on the compressional side, because right-lateral mode II rupture entering the intersection produces incremental extensional or compressional stress on the two sides (Figure 4c).

2.5. Numerical Implementation of Spontaneous Rupture

[19] In order to nucleate dynamic rupture, we first assume a nucleation zone in a static equilibrium state on the planar main fault using the elastostatic BIEM whose slip satisfies the slip-weakening boundary condition (Appendix A). In practice, we determine an initial static equilibrium configuration for which slip is allowed within a region of length $L_c' = 12R_0$, slightly larger than $L_c = (64/9\pi^2) [(0.6 - 0.12)/(0.24 - 0.12)]^2 R_0 \approx 11.53R_0$ in equation (3), but prevent slip outside that region. That causes an initial stress concentration which is slightly larger than the peak strength at the both tips of the static nucleation zone, and finitely accelerates rupture in the first dynamic time steps.

[20] At the time step zero, we begin dynamic rupture from both ends. Spatiotemporal rupture evolution is determined by the following time marching procedure: In every time step, we first determine the rupturing regions at that step on both faults. We evaluate the shear traction at each rupture tip and judge whether it extends or not by comparing the traction with the peak strength at the same position. For rupture on a planar main fault, we always do so at both tips. For rupture on a branching fault, we keep monitoring stress at all time steps at the first element of the branching fault, originating from the intersection, until nucleation occurs there. After nucleation we do the same at the tip of the branching rupture. We then determine the slip velocity on the rupturing region(s) by solving the coupled equations (1) and (4). On either branch the peak stress depends on the total normal stress as shown in equation (2), which will be altered interactively by rupture on the other branch.

[21] To explain that solution procedure, we write the constitutive relation of equation (1) as $\tau = f(\Delta u)(-\sigma_n)$ when the slip rate $V > 0$, and $\tau \leq f(\Delta u)(-\sigma_n)$ when $V = 0$, where the function $f(\Delta u)$ describes the slip weakening from μ_s to μ_d like in equations (1) and (2) and Figure 2b. Here $V < 0$ is prohibited and we assume $\sigma_n < 0$. We choose the slip rate V^{lm} in each cell l during time step m to assure that the constitutive relation is satisfied by the stresses τ^{lm} and σ_n^{lm}, and slip $\Delta u^{lm} = \Delta u^{l\,(m-1)} + V^{lm}\Delta t$, at the end of that time step. We can write $\tau^{lm} = \tau_{V=0}^{lm} - \mu V^{lm}/2c_s$ where $\tau_{V=0}^{lm}$ is the part of τ^{lm} that would be calculated by using $V^{lm} = 0$ in equation (4) for $\Delta\tau^{lm}$; like is also the case for σ_n^{lm}, the term $\tau_{V=0}^{lm}$ depends only on the slip history prior to time step m.

[22] Thus if $\tau_{V=0}^{lm} < f(\Delta u^{l(m-1)})\,(-\sigma_n^{lm})$, we take $V^{lm} = 0$ and set $\Delta u^{lm} = \Delta u^{l(m-1)}$. If otherwise, we solve for V^{lm} in

$$\tau_{V=0}^{lm} - \mu V^{lm}/2c_s = f\left(\Delta u^{l(m-1)} + V^{lm}\Delta t\right)\left(-\sigma_n^{lm}\right). \quad (5)$$

That is seen (by sketching both sides as a function of V^{lm}) to always have a unique solution which lies in the range $V^{lm} \geq 0$ provided that the maximum value of $-df(\Delta u)/d(\Delta u)$, which is $(\mu_s - \mu_d)/D_c$ in our case, satisfies

$$\mu/2c_s > \left(-\sigma_n^{lm}\right)\Delta t(\mu_s - \mu_d)/D_c. \quad (6)$$

For our case the nominal size of the low-speed slip-weakening zone, given as above with $\tau_p - \tau_r = (\mu_s - \mu_d)(-\sigma_n)$ and $G = (\mu_s - \mu_d)(-\sigma_n)D_c/2$, is $R_0 = (3\pi/8)\mu D_c/[(\mu_s - \mu_d)(-\sigma_n)]$, and we take $\Delta t = \Delta\,s/2c_d$ so that, upon multiplying by $2c_s/\mu$ and using $c_d = \sqrt{3}c_s$, the inequality assuring a unique solution for V^{lm} becomes $1 > (\sqrt{3}\pi/8)\Delta s/R_0 \approx 0.7\,\Delta s/R_0$. That will be met by a wide margin if the mesh is sufficiently refined to keep the grid spacing Δs small compared to R_0, which is also a basic requirement for spatial resolution of the solution.

[23] We choose R_0, the nominal size at low speed of the slip-weakening zone based on the normal prestress $-\sigma_{yy}^0$ on the main fault, as a basic size scale, following *Poliakov et al.* [2002]. In the computations, we choose Δs fine enough to tolerably resolve the slip-weakening zone size R even at the high-speed propagation stage (as mentioned before, R decreases with v_r). For that we take $\Delta s = R_0/5$ for the low and the intermediate velocities $v_r = 0.6c_s$ and $0.8c_s$ and $\Delta s = R_0/10$ for the high velocity $v_r = 0.9c_s$. Again, the time step interval Δt is chosen as $c_d\Delta t/\Delta s = 1/2$ to satisfy causality. We confirmed that R is well resolved in the computations and occupies about 4 grid spacings at the high velocity of $v_r = 0.9c_s$ as is expected from the theoretical analysis [*Rice*, 1979]. We also take R_0/c_d as a basic timescale and $(-\sigma_{yy}^0)$ as a stress scale. Thus only dimensionless ratios are used in the computations.

[24] We introduce an artificial damping term to eliminate a short-wavelength oscillation in slip velocity that otherwise slowly becomes evident as the time steps increase and then grows rapidly to the point of invalidating the solution (see Appendix B).

3. Dynamically Self-Chosen Path on a Branched Fault System

[25] We systematically investigated the dynamically self-chosen path on branched faults for all parameter combina-

tions (48 simulations: 4 prestress states $\times$ 3 rupture velocities $\times$ 4 branching angles). From these results, here we discuss 5 typical examples in which we can elicit the characteristic effects of prestress state, rupture velocities and branch angle on dynamic branching. The final paths in the vicinity of the branch intersections are summarized in section 3.2.

3.1. Effect of Prestress State

[26] By comparing results for different S_{max} inclinations in the prestress state ($\Psi = 56°$, $25°$ and $13°$), we can see the effect of prestress state. Here we choose low rupture velocity ($v_r = 0.6c_s$) to reduce the effect of dynamic off-fault stressing as shown in Figure 1, and we begin with narrow branching angle in order to contrast the results with that with wide angle later.

3.1.1. Case With High Inclination of S_{max}, $\Psi = 56°$

[27] Figure 5 shows the snap shots of spontaneous rupture propagation for the case with high inclination of S_{max}, $\Psi = 56°$. Rupture nucleates on the main fault at $c_d(t/R_0) = 0.0$, and its velocity accelerates to $v_r = 0.6c_s$ in reaching the intersection with a narrow branch ($\varphi = -15°$) on the extensional side. Figure 5 (right) shows detailed snapshots after the rupture front passes the intersection. Rupture first transfers on the extensional branch at $c_d(t/R_0) = 35.7$. It is then running on both branches for awhile ($c_d(t/R_0) = 35.9$, 36.6). However, this does not last long and rupture on the extensional branch comes to dominate. After that, rupture on the main branch is terminated ($c_d(t/R_0) = 46.4$). Finally, rupture on the extensional branch is the dynamically self-chosen path ($c_d(t/R_0) = 54.5$).

[28] Here we can interpret the result that the extensional branch is dynamically self-chosen in terms of the prestress state and the branching angle. In this case, the prestress state is more favorable on the extensional branch than on the main branch (see Figure 4a). The peak fracture strength that controls rupture nucleation is $\tau_p^0/(-\sigma_{yy}^0) = 0.60$ on the main branch and $\tau_p^b/(-\sigma_{yy}^0) = 0.54$ on the extensional branch. This means the extensional branch is more favorable to nucleate rupture. In addition, the stress drop, an essential factor for rupture continuation, is $\Delta\sigma^0/(-\sigma_{yy}^0) = 0.12$ on the main branch and $\Delta\sigma^b/(-\sigma_{yy}^0) = 0.15$ on the extensional branch. This means the extensional branch is more favorable to encourage rupture to continue. That is, the extensional branch is more favorable than the main branch both for rupture nucleation and for continuation. Although this consideration is limited only to the prestress state, omitting the stress contribution due to running rupture, it is helpful as a starting point for our interpretation. When we take the incremental stresses due to rupture into consideration as we actually do in the computations, the extensional branch is much more favorable: Rupture entering the intersection produces incremental extensional stress on the extensional side and this induces a lower peak strength and larger stress drop on the extensional branch due to significant decrease of total normal stress. This contributes additionally to rupture on the extensional side being dynamically self-chosen.

[29] This advantageous condition on the extensional branch itself does not answer why only the branch is finally chosen. We can interpret that in terms of stress interaction between branches. In Figure 5, we can see simultaneous
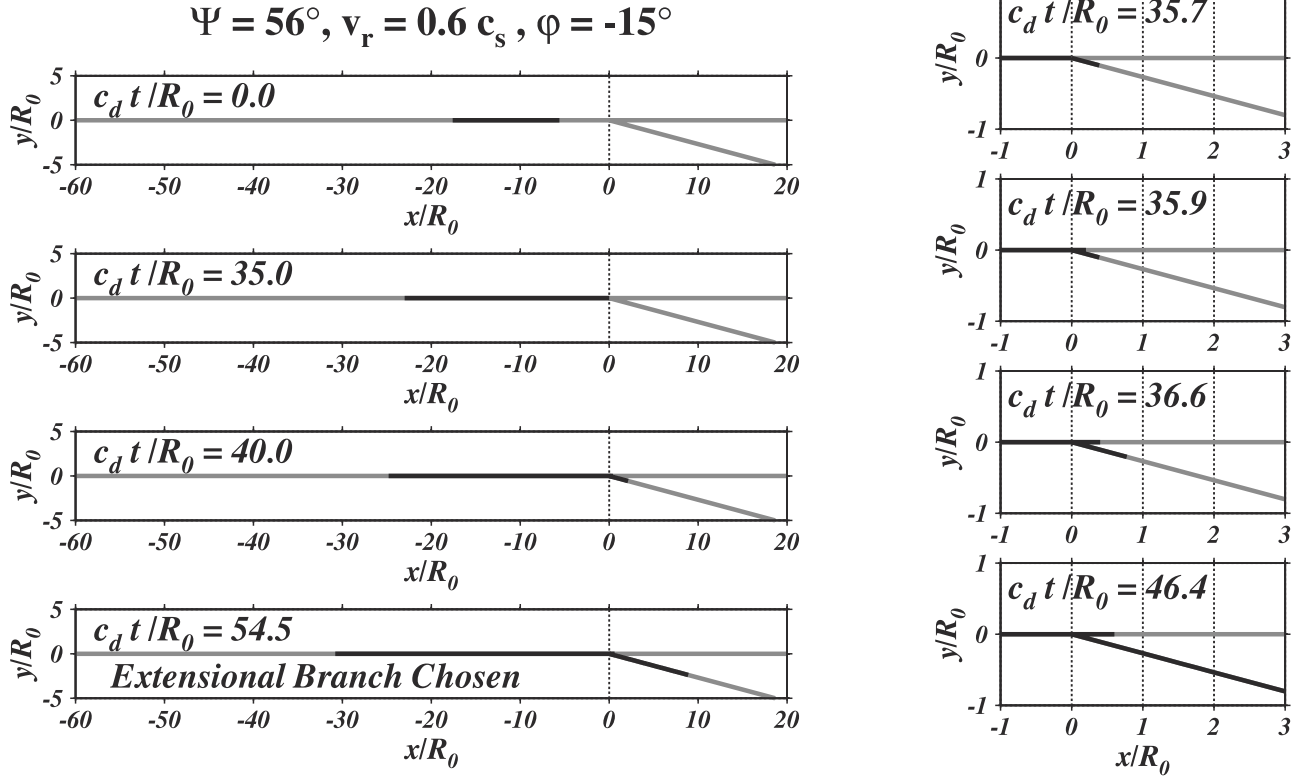
Figure 5. (left) Snap shots of spontaneous rupture propagation for a case with high inclination of S_{max}, $\Psi = 56°$, low rupture velocity, $v_r = 0.6c_s$, and narrow branch angle in the extensional side, $\varphi = -15°$. (right) Detailed snap shots in the vicinity of the branch intersection.

rupture on both branches (at $c_d(t/R_0) = 35.9$, 36.6) for a while. During this, rupture on the extensional branch is promoted more than on the main branch due to better conditions on it. Accordingly rupture on the extensional branch begins to prevail. Once rupture prevails on the extensional branch, the shear stress around the fractured surface is released and rupture on the other branch becomes difficult to continue for lack of energy release: The rupture tip of the main branch is covered by this decreased stress zone, named "stress shadow" zone, and thus no longer is encouraged by the surrounding stress field. This is we think why the main rupture is finally arrested. The result that rupture on the extensional branch is dynamically self-chosen can be attributed to the effect of high inclination of S_{max} in the prestress state and narrow branching angle. As to the rupture velocity change across the intersection, the rupture velocity v_r immediately increases up to the limiting velocity c_R on the extensional branch encouraged by greater stress drop on it.

3.1.2. Case With Intermediately Low Inclination of S_{max}, $\Psi = 25°$

[30] The snap shots for this case are shown in Figure 6. Spontaneous rupture begins at $c_d(t/R_0) = 0.0$ and the rupture velocity accelerates up to $0.6c_s$ at $c_d(t/R_0) = 35.0$ in reaching the intersection point with an extensional narrow branch ($\varphi = -15°$). In this case, rupture bifurcates on both branches at the same time ($c_d(t/R_0) = 35.6$ in Figure 6 (right)). Rupture on the extensional branch is, however, soon termi-

nated ($c_d(t/R_0) = 36.7$) and rupture only on the main branch continues to propagate ($c_d(t/R_0) = 46.4$). In this case, rupture on the main branch is dynamically self-chosen.

[31] We can understand this result because the prestress state is more favorable on the main branch (see Figure 4a). Especially, stress to be released based on the prestress state is $\Delta\sigma^0/(-\sigma_{yy}^0) = 0.12$ on the main branch and $\Delta\sigma^b/(-\sigma_{yy}^0) = -0.00$ on the extensional branch. This means that rupture on the extensional branch has no drive to continue and soon terminates, although it could be dynamically nucleated by the local stress concentration of the approaching rupture front. The result that rupture on the main branch is dynamically chosen can be attributed mainly to the effect of intermediately low inclination of S_{max} in the prestress state. As to the rupture velocity, no significant velocity change is observed across the intersection. v_r smoothly speeds up to c_R on the main branch.

3.1.3. Case With Low Inclination of S_{max}, $\Psi = 13°$

[32] The snap shots for this case are shown in Figure 7. Spontaneous rupture begins at $c_d(t/R_0) = 0.0$ and the rupture velocity accelerates up to $0.6c_s$ at $c_d(t/R_0) = 35.0$ in entering the intersection point with a compressional narrow branch ($\varphi = +15°$). Rupture bifurcates on both branches at the same time $c_d(t/R_0) = 35.6$. Then rupture on the compressional branch is promoted more than on the main branch ($c_d(t/R_0) = 36.1$). Rupture on the main branch is terminated ($c_d(t/R_0) = 36.6$) and rupture on the compressional branch finally prevails ($c_d(t/R_0) = 46.4$). In this case, rupture on the compressional branch is dynamically self-chosen.
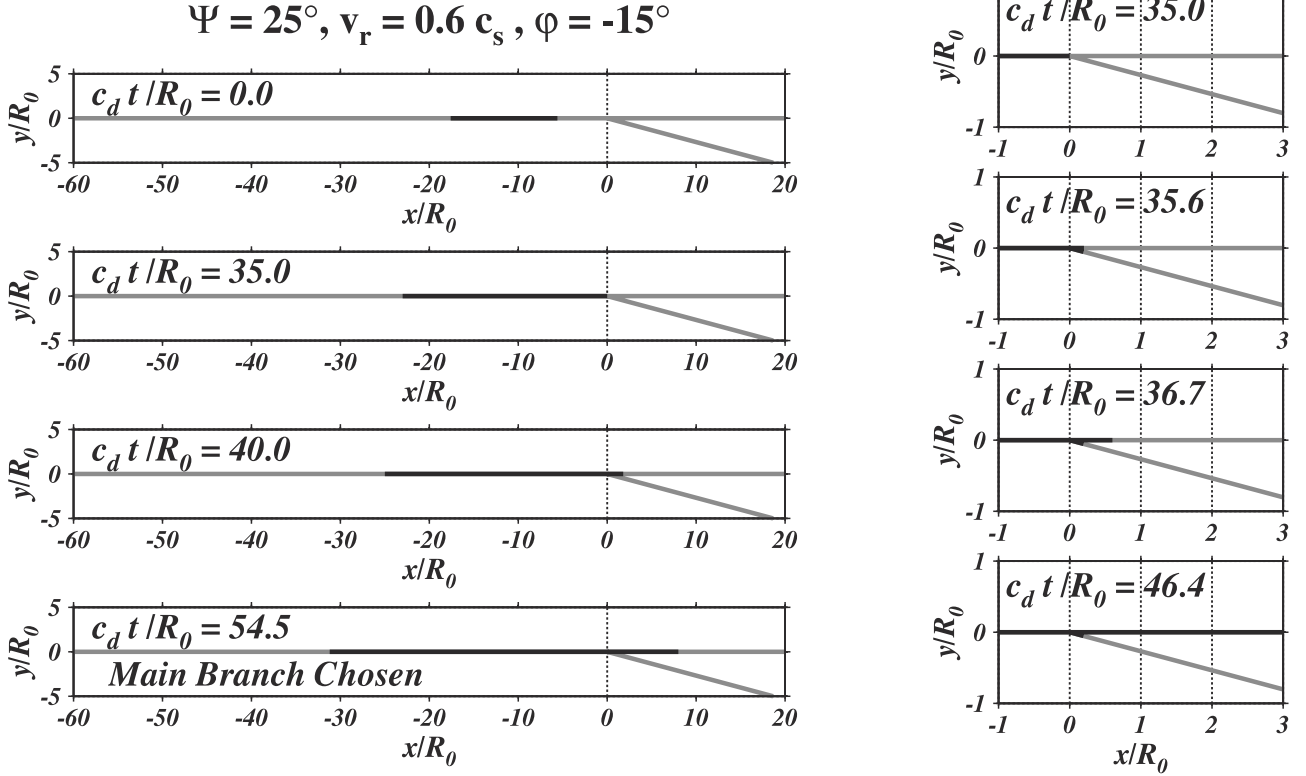
$\Psi = 25°$, $v_r = 0.6\,c_s$, $\varphi = -15°$

Figure 6. (left) Snap shots of spontaneous rupture propagation for a case with intermediately low inclination of S_{max}, $\Psi = 25°$, low rupture velocity, $v_r = 0.6c_s$, and narrow branch angle in the extensional side, $\varphi = -15°$. (right) Detailed snap shots in the vicinity of the branch intersection.

[33] In this case, the compressional branch is in a more favorable direction of the two in the prestress state (see Figure 4a). Strikingly, stress drop in the prestress state is $\Delta\sigma^b/(-\sigma_{yy}^0) = 0.31$ on the compressional branch, which is about 2.5 times greater than that on the main branch ($\Delta\sigma^0/(-\sigma_{yy}^0) = 0.12$). The peak fracture strength is not favorable on the compressional branch, $\tau_p^b/(-\sigma_{yy}^0) = 0.71$ is a little larger than the main branch ($\tau_p^0/(-\sigma_{yy}^0) = 0.60$). Despite this, rupture on the compressional branch is successfully nucleated by stress changes at the propagating rupture tip. After bifurcation, rupture on the compressional branch is promoted more due to greater stress drop on it. Rupture accelerates rapidly on it and finally prevails, and rupture on the main branch terminates as it becomes covered with the stress shadow. The result that rupture on the compressional branch is chosen can be attributed to the effect of the low inclination of S_{max} in the prestress state and the narrow branching angle.

[34] A significant factor in this case is that rupture velocity on the compressional branch exceeds c_s and speeds up to c_d, so that it is a case of super shear rupture velocity. This occurs because a fracture parameter $(\tau_p - \tau^0)/(\tau^0 - \tau_r)$, which controls the upper limit of rupture velocity in a slip-weakening model [*Andrews*, 1976], changes from 3 on the main branch to 0.8 on the compressional branch. The value 0.8 is consistent with the super-shear rupture propagation condition shown by *Andrews* [1976].

[35] After the three simulations, we can briefly summarize the effect of the prestress state and the branching angle:

The dynamically self-chosen path switches from the extensional side to the compressive side as we consider progressively shallower angle of the direction of maximum precompression with the main planar fault. Because of stress interaction between branches, only one branch is dynamically self-chosen on branched faults with narrow branching angles when rupture velocity entering the intersection is low.

3.2. Effect of Rupture Velocity at the Intersection

[36] By comparing results for $v_r = 0.6c_s$, $0.8c_s$ and $0.9c_s$ under the same inclination of S_{max} (cases with high inclination $\Psi = 56°$), we will see the effect of rupture velocity. We can expect increasing off-fault stressing for the higher rupture velocity [see *Kame and Yamashita*, 1999a, 1999b; *Poliakov et al.*, 2002]. Accordingly, rupture on both branches can possibly be driven even for a narrow branching angle. To investigate this, we consider the extensional narrow branch ($\varphi = -15°$) under three different rupture velocities. We have already seen that simultaneous rupture on both branches failed due to stress interaction for the low rupture velocity $v_r = 0.6c_s$ with narrow branching angle ($\varphi = -15°$).

3.2.1. Case With Low Rupture Velocity, $v_r = 0.6c_s$

[37] The snap shot of this case has already been shown in Figure 5. As mentioned above, rupture on the extensional branch is dynamically self-chosen for $v_r = 0.6c_s$ both due to high inclination of S_{max} in the prestress state and due to narrow branching angle. Note that rupture on the main
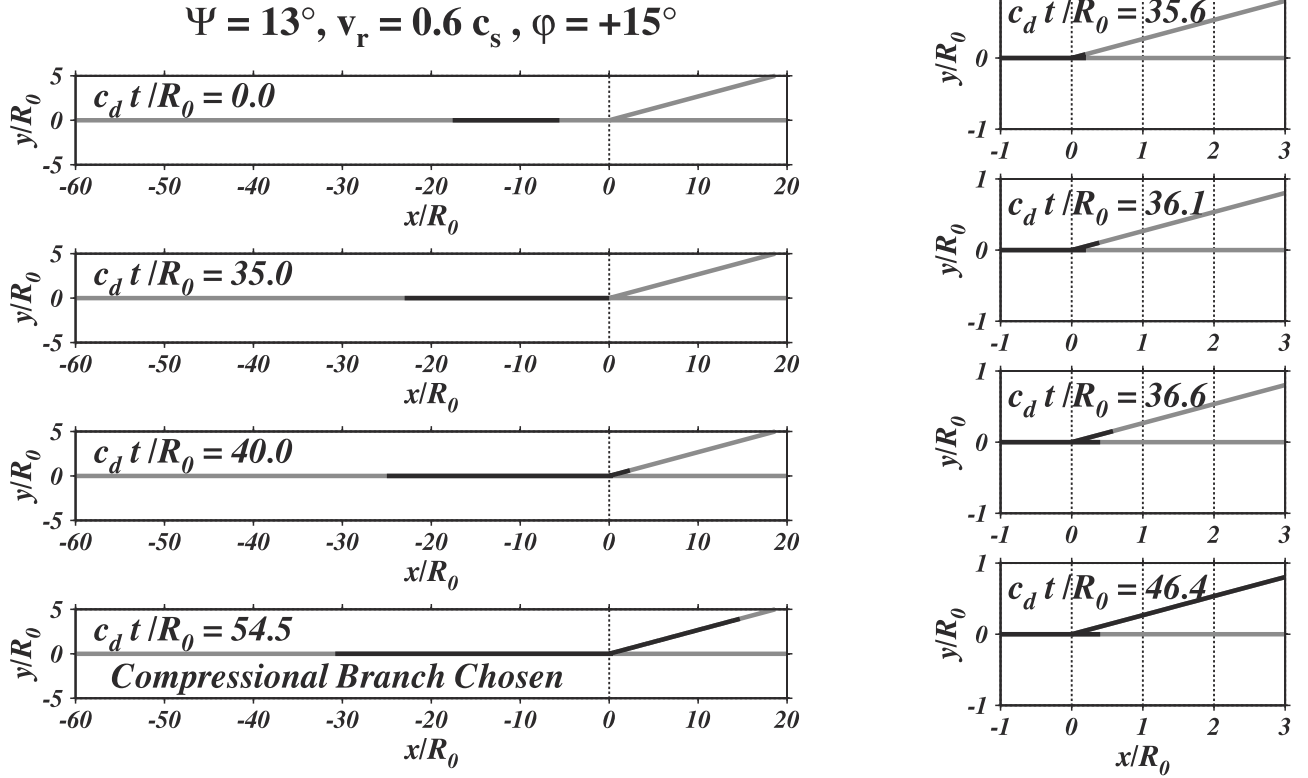
Figure 7. (left) Snap shots of spontaneous rupture propagation for a case with low inclination of S_{max}, $\Psi = 13°$, low rupture velocity, $v_r = 0.6c_s$, and narrow branch angle in the compressional side, $\varphi = +15°$. (right) Detailed snap shots in the vicinity of the branch intersection.

branch is terminated after propagating by a distance of $0.6R_0$ from the intersection.

3.2.2. Case With Intermediate Rupture Velocity, $v_r = 0.8c_s$

[38] In this case, rupture on the extensional side is dynamically self-chosen too. However, rupture on the main branch could grow more a length of $1.4R_0$ due to the enhanced dynamic stress field at higher v_r.

3.2.3. Case With High Rupture Velocity, $v_r = 0.9c_s$

[39] The snap shots for high rupture velocity are shown in Figure 8. At $c_d(t/R_0) = 0.0$, rupture nucleates to grow spontaneously and then the rupture velocity v_r accelerates to $0.6c_s$, $0.8c_s$ and $0.9c_s$ at $c_d(t/R_0) = 35.0$, 59.1 and 92.8 respectively. At the intersection, rupture first transfers to the extensional branch ($c_d(t/R_0) = 92.9$). In this case, simultaneous rupture on both branches continues although rupture on the extensional branch precedes all the time ($c_d(t/R_0) = 93.4$, 96.0 and 98.0). Simultaneous rupture on both branches lasts long and, apparently, finally succeeds to propagate forever ($c_d(t/R_0) = 120.0$), that is, rupture on both branches is dynamically self-chosen.

[40] Once two rupture fronts are sufficiently away from each other, the interaction is no longer effective in stopping rupture on the other branch. We know that both branches are good for rupture continuation ($\Delta\sigma^0/(-\sigma_{yy}^0) = 0.12$, $\Delta\sigma^b/(-\sigma_{yy}^0) = 0.15$). As to the rupture velocity across the intersection point, v_r on the main branch slows down a little after bifurcation ($c_d(t/R_0) = 93.4$) because of the stress shadow of the extensional branch. However, it again speeds up to c_R as it separates from the extensional branch. On the

other hand, v_r on the extensional branch just speeds up to c_R as encouraged by the surrounding stress.

[41] In the above three simulations, we can see the significant effect of rupture velocity: The dynamic stressing around a propagating rupture is enhanced with increasing rupture velocity. That can drive rupture on both branches a little longer for the case with $v_r = 0.8c_s$, or can drive rupture on both branches to extend indefinitely for the case with $v_r = 0.9c_s$, very near the limiting velocity (Rayleigh wave velocity for mode II, which is $0.92c_s$).

3.3. Effect of Branching Angle

[42] By comparing results for $\varphi = -15°$ and $\varphi = -30°$ under the same inclination of S_{max} (cases with $\Psi = 56°$), and under the same rupture velocity ($v_r = 0.6c_s$), we will see the effect of the branching angle. For the wide branching angle ($\varphi = -30°$), we can expect rupture on both branches to be less affected by stress interaction.

3.3.1. Case With Narrow Branching Angle, $\varphi = -15°$

[43] The snap shots has already been shown in Figure 5. Both branches are favorable for rupture to continue with positive stress drop on them ($\Delta\sigma^0/(-\sigma_{yy}^0) = 0.12$ on the main branch and $\Delta\sigma^b/(-\sigma_{yy}^0) = 0.15$ on the extensional branch). However, rupture only on the extensional branch is dynamically self-chosen due to strong stress interaction for the narrow branching angle ($\varphi = -15°$).

3.3.2. Case With Wide Branching Angle, $\varphi = -30°$

[44] The snap shots for the wide branching angle are shown in Figure 9. At $c_d(t/R_0) = 0.0$, rupture nucleates to grow spontaneously and then the rupture velocity v_r accel-
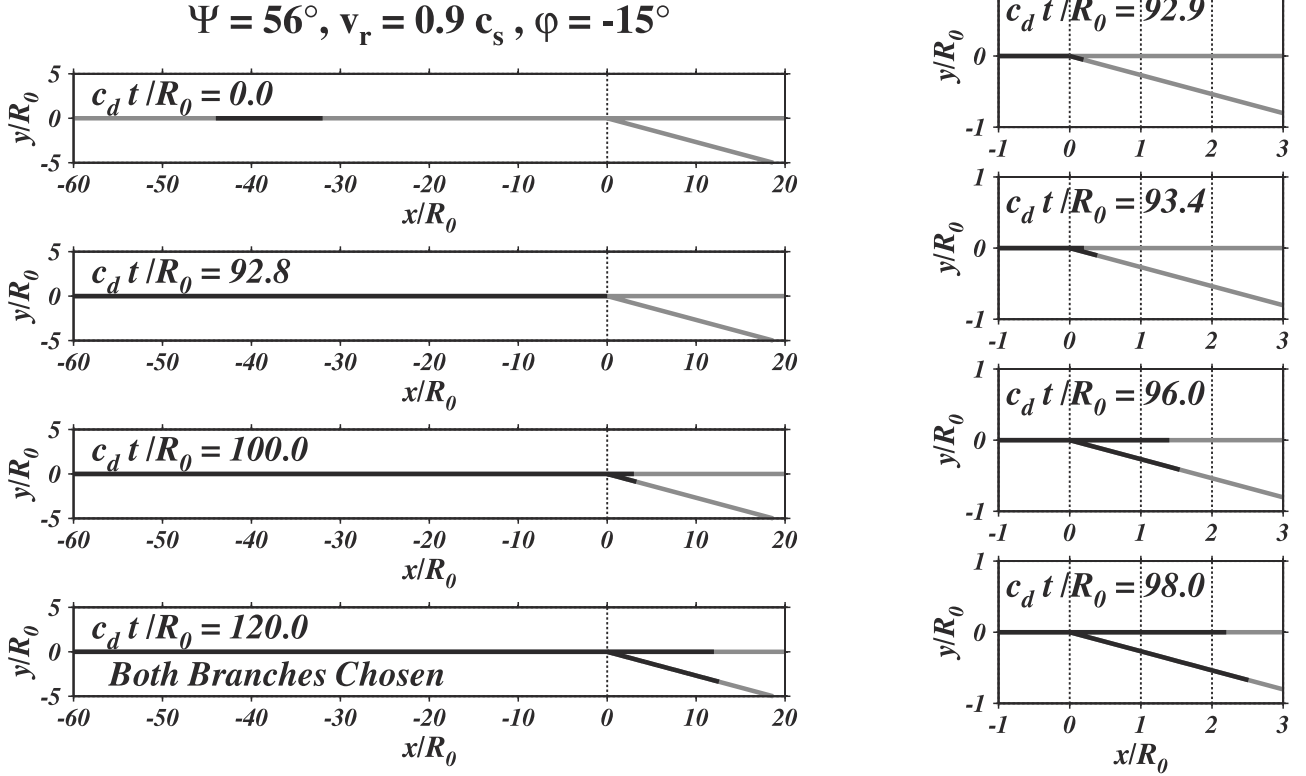
Figure 8.   (left) Snap shots of spontaneous rupture propagation for a case with high rupture velocity, $v_r = 0.9 c_s$, high inclination of S_{max}, $\Psi = 56°$, and narrow branching angle in the extensional side, $\varphi = -15°$. (right) Detailed snap shots in the vicinity of the branch intersection.

erates to $0.6 c_s$ at $c_d(t/R_0) = 35.0$. At the intersection, rupture first transfers to the extensional branch at $c_d(t/R_0) = 35.4$. In this case, simultaneous rupture on both branches can continue although rupture on the extensional branch proceeds all the time ($c_d(t/R_0) = 36.8, 38.2, 39.6$). Simultaneous rupture finally succeeds to propagate forever ($c_d(t/R_0) = 54.5$), that is, rupture on both branches is dynamically self-chosen.

[45] In this case, both branches are also favorable for rupture to continue, the same as for the narrow branching model. The stress drop is $\Delta\sigma^0/(-\sigma^0_{yy}) = 0.12$ on the main branch and $\Delta\sigma^b/(-\sigma^0_{yy}) = 0.12$ on the extensional branch. In contrast to the case with the narrow branching angle ($\varphi = -15°$), rupture once nucleated on both branches can continue forever due to weaker stress interaction in the wide branching angle ($\varphi = -30°$), even when the rupture velocity v_r upon reaching the intersection is low ($v_r = 0.6 c_s$).

4.   All Simulation Results

[46] In this section, we show all the simulation results and answer the following questions: Does the rupture start along the branch? Does it continue? Which side is most favored for branching, the extensional or compressional? Does rupture continue on the main fault too? What path is finally self-chosen? The final paths in the vicinity of intersection are summarized for each S_{max} inclination. They are final and will not change with time after the propagating rupture tip(s) has(have) gone away from the intersection at the times shown in the diagrams. Stress drop and peak strength, based

on "the prestress state" on each branch, are noted for reference. Note that the rupture paths are all chosen by the total stress, a sum of the prestress and the incremental stress, which is altered dynamically by interacting rupture on the faults.

4.1.   Case With High Inclination of S_{max}, $\Psi = 56°$

[47] Diagram of final rupture traces is shown in Figure 10 and the most favored angle for the prestress state is $-15°$, on the extensional side (see Figure 4a). (1) On the compressional side, rupture on the branching fault is not chosen because it is not on the favorable side although nucleation there could be excited dynamically for high rupture velocity (cases with $v_r = 0.9 c_s$). (2) On the extensional side, for cases with the narrow angle, $\varphi = -15°$, rupture on the extensional branch is dynamically self-chosen for low rupture velocity. However, rupture on both branches becomes possible as rupture velocity approaches the high velocity, $0.9 c_s$. For cases with the wide-angle, $\varphi = -30°$, rupture on both branches is dynamically self-chosen at all v_r.

4.2.   Case With Intermediate Inclination of S_{max}, $\Psi = 45°$

[48] Diagram of final rupture traces is shown in Figure 11 and the most favored angle for the prestress state is $-3°$, on the extensional side (see Figure 4a). (1) On the compressional side, rupture on the main fault is always self-chosen because the compressional branch is not in the favorable side though nucleation on it could be excited dynamically for high rupture velocity (cases with $v_r = 0.9 c_s$). (2) On the
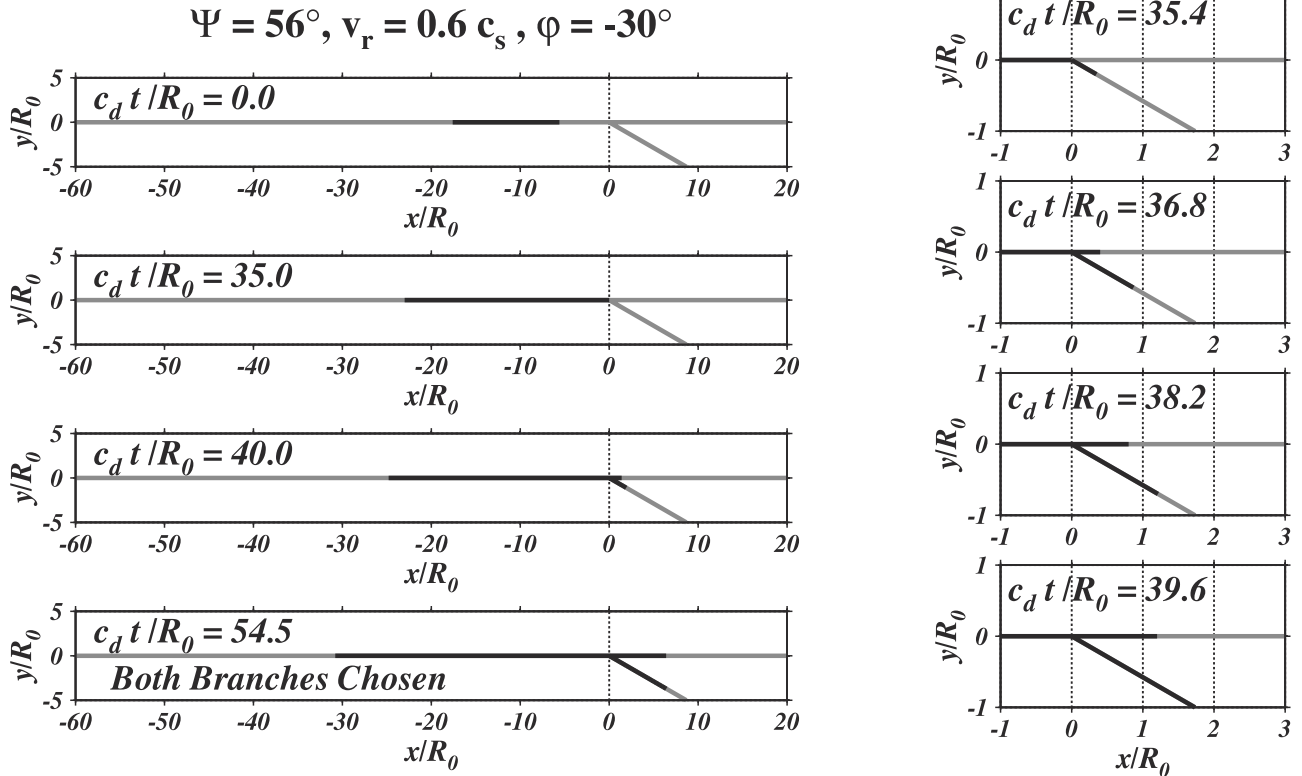
$$\Psi = 56°, \; v_r = 0.6 \, c_s, \; \varphi = -30°$$

Figure 9. (left) Snap shots of spontaneous rupture propagation for a case with wide branching angle in the extensional side, $\varphi = -30°$, low rupture velocity, $v_r = 0.6c_s$, and high inclination of S_{max}, $\Psi = 56°$. (right) Detailed snap shots in the vicinity of the branch intersection.

extensional side, the main branch is basically self-chosen and simultaneous rupture on both branches becomes possible as the rupture velocity approaches $0.9c_s$. An exception is the case with low rupture velocity, $v_r = 0.6c_s$, and narrow branching angle, $\varphi = -15°$. In this case, a more favorable condition is temporarily attained on the extensional branch by the propagating rupture tip. The temporary advantage is lost when dynamic stressing is high enough, at the higher v_r, to encourage rupture on the main branch whose stress drop is originally greater than the branching fault. Note that failed, or stopped, branches are generally longer in this $\Psi = 45°$ case than for $\Psi = 56°$.

4.3. Case With Intermediately Low Inclination of S_{max}, $\Psi = 25°$

[49] Diagram of final rupture traces is shown in Figure 12 and the most favored angle for the prestress state is $+16°$, on the compressional side (see Figure 4a). For this prestress state, the main branch is dynamically self-chosen for all cases although rupture on the branching fault becomes nucleated as rupture velocity increases. (1) On the compressional side, the branching fault is on the compressional, favored side. However, the peak strength is greater especially when rupture is entering the intersection due to incremental compressional stressing. In these cases, rupture on the branching fault is nucleated not at but behind the rupture front, that is, the nucleation occurs after rupture front on the main fault passed by the intersection, that is, branching behind. It is aided by high off-fault stressing

behind the propagating rupture tip. Accordingly, rupture once nucleated on the branching fault is soon arrested by the stress shadow of the main fault just after dynamic stress waves pass through the intersection. (2) On the extensional side, the branching fault is not on the favored side (stress drops are negative). Accordingly rupture on the extensional branch is just nucleated dynamically but soon arrested by the lack of stress release on it. Note that for high rupture velocity, branches are generally longer on the extensional side although the most favored angle is on the compressional side. That "favored" angle is, however, based only on the prestress state, whereas the rupture paths are chosen by the total stress. The incremental stress, which is always favorable to the extensional side, is enhanced with increasing rupture velocity and the total stress thus becomes favorable temporarily to the extensional side. We think that is why branches are longer on the extensional side.

4.4. Case With Low Inclination of S_{max}, $\Psi = 13°$

[50] Diagram of final rupture traces is shown in Figure 13 and the most favored angle for stress drop is $+29°$, on the compressional side (see Figure 4a). (1) On the compressional side, for the wide branching angle, secondary rupture is nucleated behind the rupture tip on the main fault owing to greater peak strength on the branching fault. When rupture velocity is low, off-fault stressing is not high enough to continue rupture on the branching fault and the weak stress shadowing from the main fault prevails. As rupture velocity increases, off-fault stresses are enhanced so that
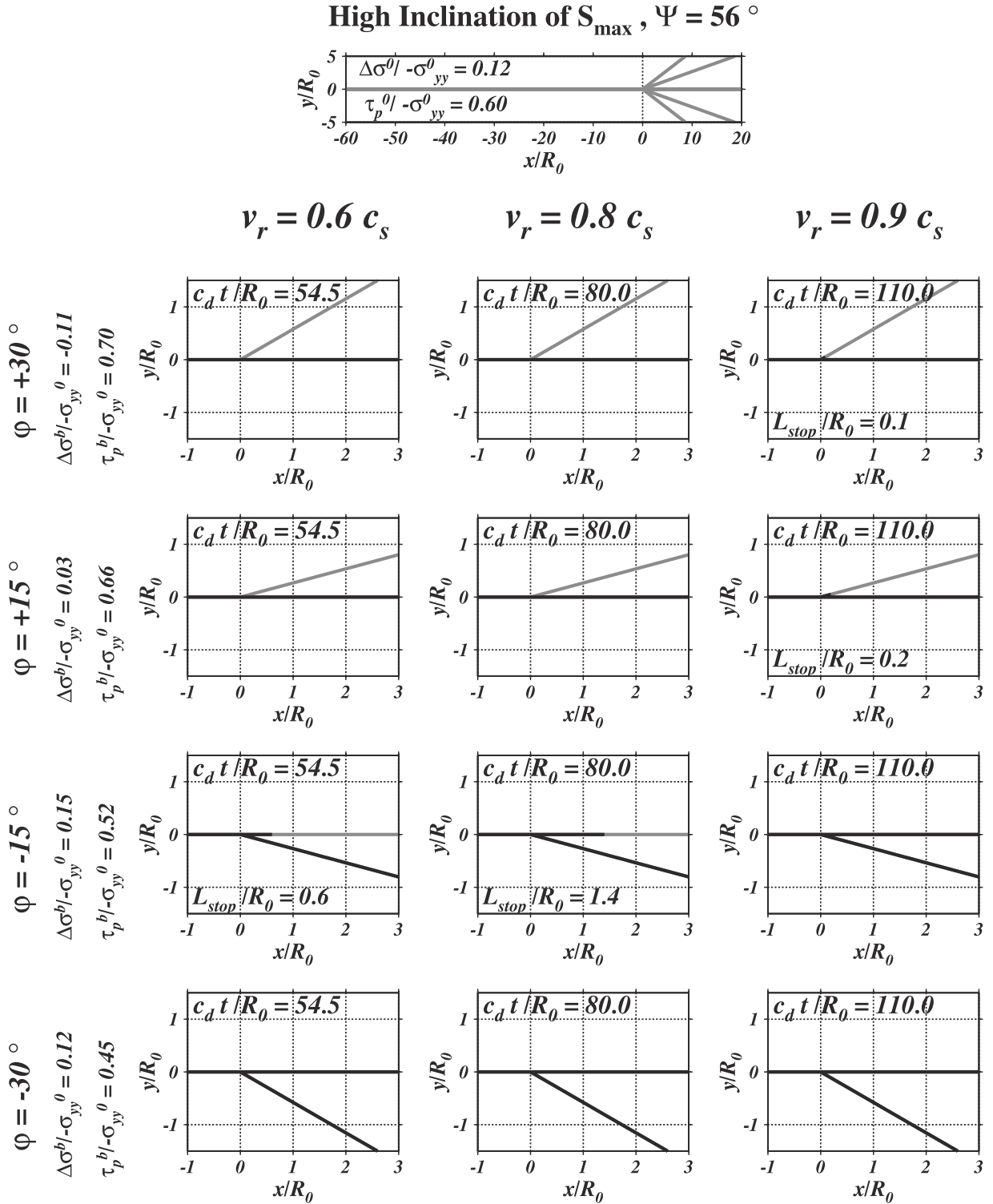
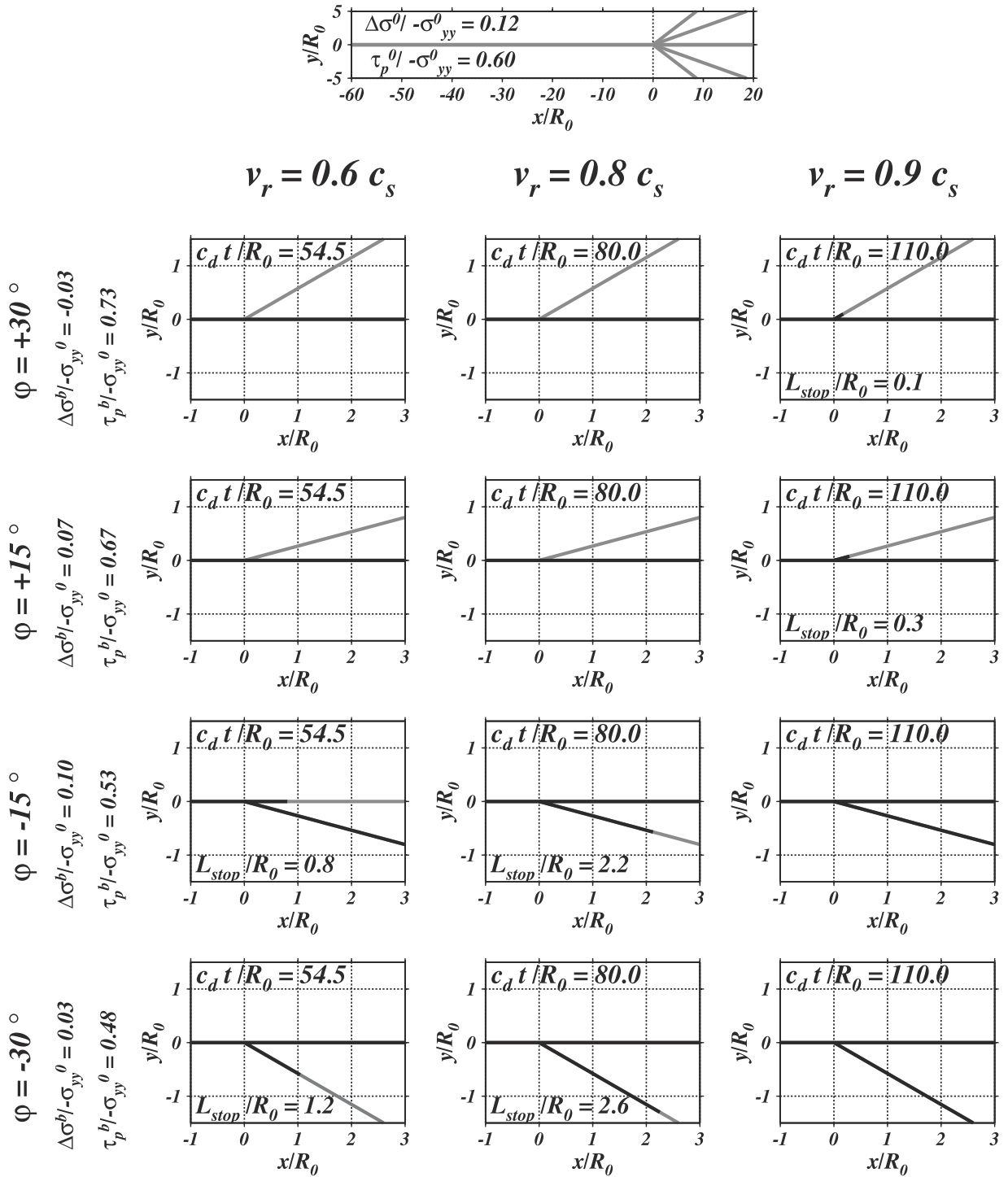**Figure 10.** Diagram of final rupture traces in the vicinity of the intersection for cases with high inclination of S_{max}, $\Psi = 56°$. L_{stop} indicates the length of arrested rupture once dynamically nucleated; those are given in terms of the slip-weakening zone size R_0 for low-speed rupture along the main fault.
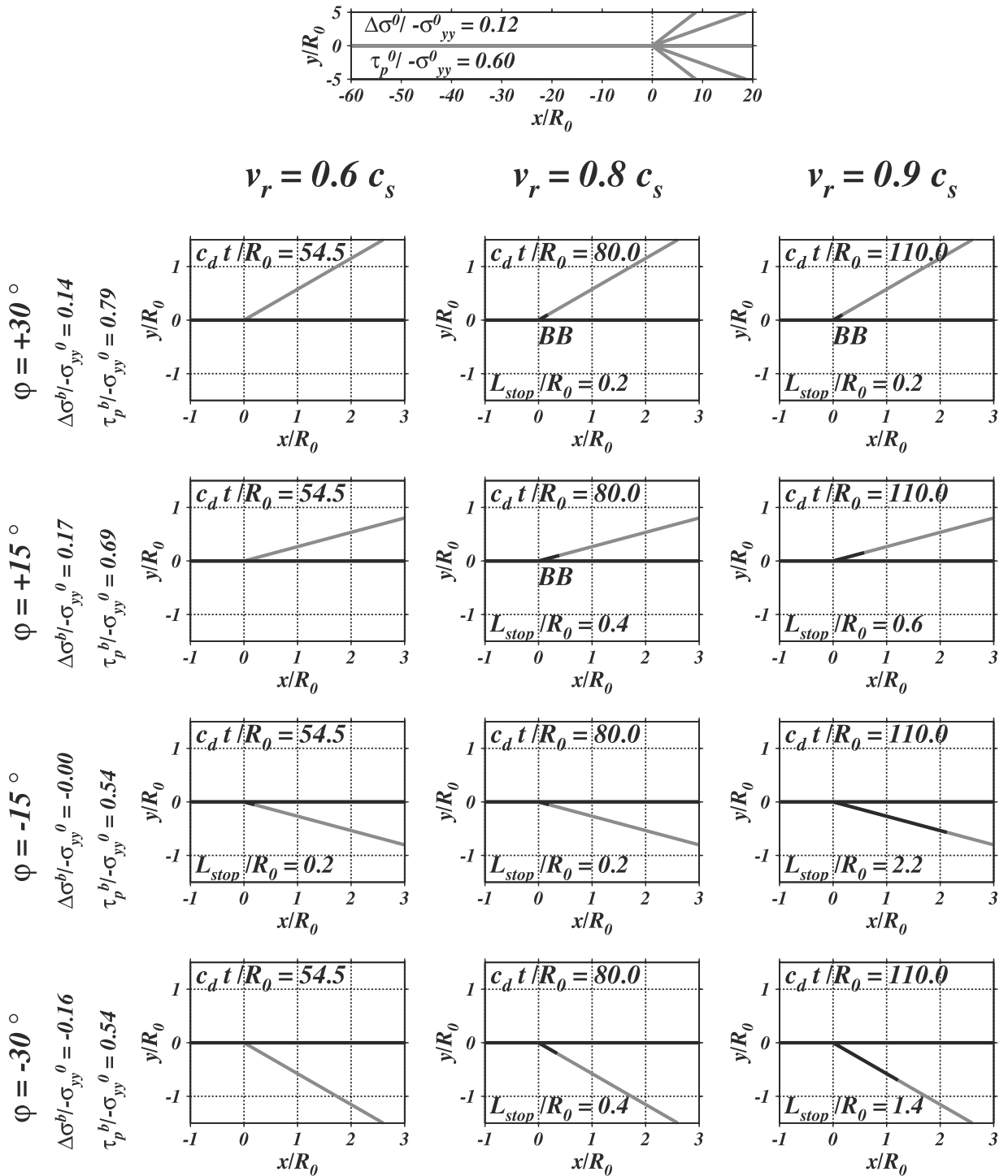
Figure 11. Diagram of final rupture traces in the vicinity of the intersection for cases with intermediate inclination of S_{max}, $\Psi = 45°$. L_{stop} indicates the length of arrested rupture once dynamically nucleated.

Intermediately Low Inclination of S_{max} , $\Psi = 25°$

Figure 12. Diagram of final rupture traces in the vicinity of the intersection for cases with intermediately low inclination of S_{max}, $\Psi = 25°$. L_{stop} indicates the length of arrested rupture once dynamically nucleated. BB indicates cases with branching behind; i.e., the rupture front on the main fault had propagated somewhat beyond the junction before slip initiated on the branch fault.
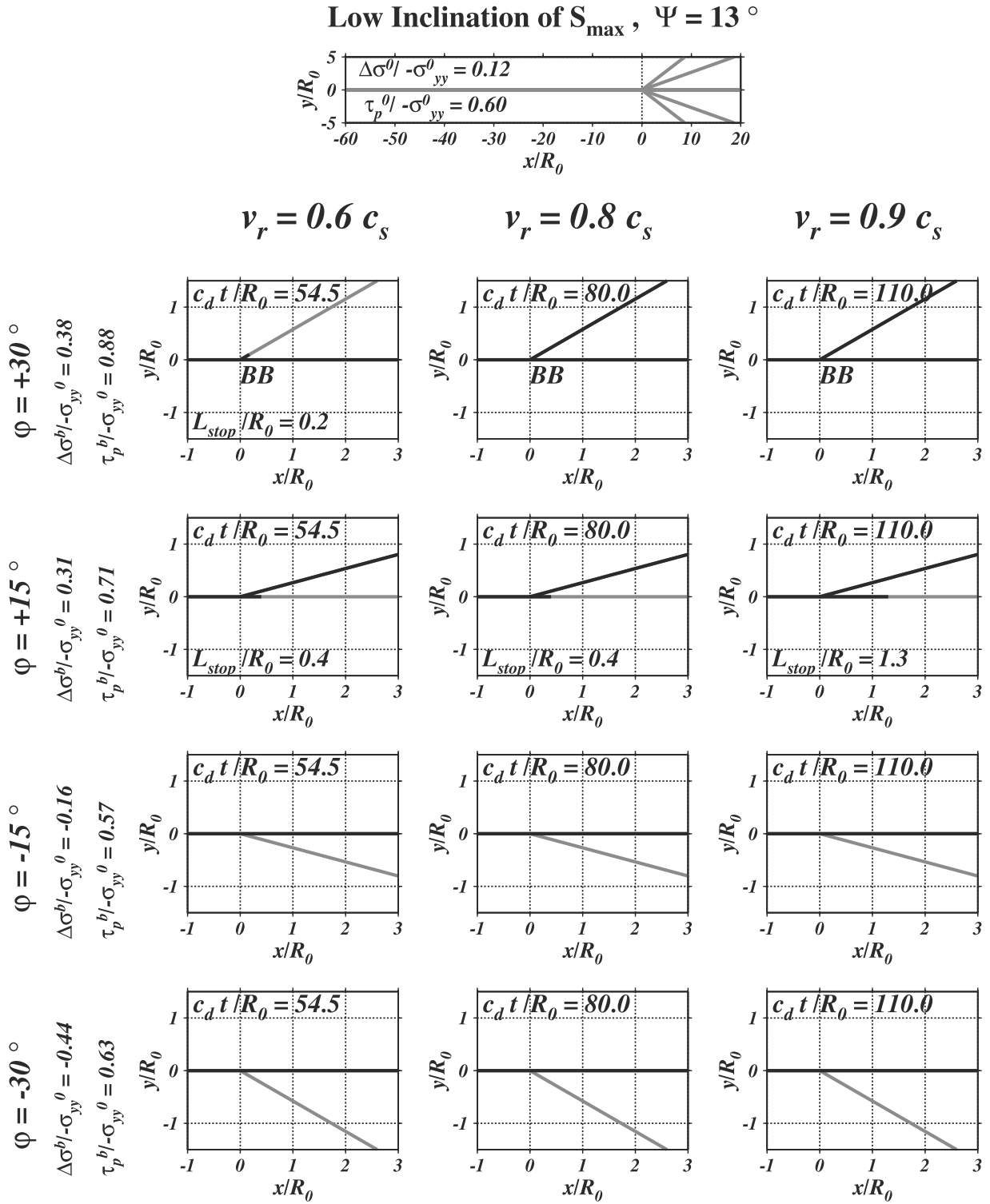
Low Inclination of S_{max} , $\Psi = 13°$

$\Delta\sigma^0/-\sigma^0_{yy} = 0.12$

$\tau_p^0/-\sigma^0_{yy} = 0.60$

$v_r = 0.6\ c_s$ $v_r = 0.8\ c_s$ $v_r = 0.9\ c_s$

$\varphi = +30°$
$\Delta\sigma^b/-\sigma^0_{yy} = 0.38$
$\tau_p^b/-\sigma^0_{yy} = 0.88$

$c_d t/R_0 = 54.5$ BB $L_{stop}/R_0 = 0.2$

$c_d t/R_0 = 80.0$ BB

$c_d t/R_0 = 110.0$ BB

$\varphi = +15°$
$\Delta\sigma^b/-\sigma^0_{yy} = 0.31$
$\tau_p^b/-\sigma^0_{yy} = 0.71$

$c_d t/R_0 = 54.5$ $L_{stop}/R_0 = 0.4$

$c_d t/R_0 = 80.0$ $L_{stop}/R_0 = 0.4$

$c_d t/R_0 = 110.0$ $L_{stop}/R_0 = 1.3$

$\varphi = -15°$
$\Delta\sigma^b/-\sigma^0_{yy} = -0.16$
$\tau_p^b/-\sigma^0_{yy} = 0.57$

$c_d t/R_0 = 54.5$

$c_d t/R_0 = 80.0$

$c_d t/R_0 = 110.0$

$\varphi = -30°$
$\Delta\sigma^b/-\sigma^0_{yy} = -0.44$
$\tau_p^b/-\sigma^0_{yy} = 0.63$

$c_d t/R_0 = 54.5$

$c_d t/R_0 = 80.0$

$c_d t/R_0 = 110.0$

Figure 13. Diagram of final rupture traces in the vicinity of the intersection for cases with low inclination of S_{max}, $\Psi = 13°$. L_{stop} indicates the length of arrested rupture once dynamically nucleated. BB indicates branching behind.

rupture on the branching fault can continue to propagate indefinitely. For the narrow branching angle, the compressional branch is successfully nucleated. It is driven by a higher stress drop than on the main fault, soon outruns it, and prevails by stress shadowing, so that it is finally self-chosen as shown in Figure 7. (2) On the extensional side, the main fault is always dynamically self-chosen.

5. Field Observations and Comparisons With Simulations

[51] Here we compare our simulation results with a set of field examples assembled for the prior, more qualitative, test of branching predictions based on the elastic stress field analysis by *Poliakov et al.* [2002]. These are shown in Figure 14 and are as follows: First we consider two continental thrust earthquakes, the 1971 San Fernando $M_L = 6.4$ and the 1985 Kettleman Hills $M_W = 6.1$ California events (Figures 14a and 14b), for which we may assume that S_{max} is horizontal. For the San Fernando earthquake, nucleation is on a steeply dipping plane of 53° dip and then rupture bends onto the 29° shallow dip plane [*Langston*, 1978; *Heaton and Helmberger*, 1979] (Figure 14a). This corresponds to a high inclination of S_{max} with the nucleation plane, $\Psi = 53°$, and branching angle $\varphi = -24°$ to the extensional side. It is consistent with the rupture path kinking to the extensional side, as shown in Figures 5, 8, 9, and 10. The 3-D models of the source process by *Heaton and Helmberger* [1979] suggest that the rupture velocity v_r was near 2.8 km/s for the deeper faulting and 1.8 km/s for the shallow fault segment. If we assume $c_s = 3.5$ km/s, typical for depths of the deeper rupture segment, $v_r = 2.8$ km/s would correspond to $v_r = 0.8 c_s$, hence to the middle column of panels in Figure 10. Because of the branching angle, $\varphi = -24°$, the comparison should be with third and fourth rows of Figure 10. We can see there that our simulations definitively predict that rupture would follow the branched path but are marginal concerning whether or not rupture would also continue along the main fault plane. Such a possibility of some continued propagation on the original fault plane has not been considered in the models of *Heaton and Helmberger* [1979]. However, if that indeed happened, the rupture did not reach the surface on that plane (in fact, we do not know in this case if how far the main fault plane actually does continue beyond the junction). Such continuation would mainly affect the records at Pacoima Dam (for the geometry of the fault rupture in relation to Pacoima Dam, see Figure 7 of *Heaton and Helmberger* [1979]).

[52] The 1985 Kettleman Hills $M_W = 6.1$ event took place on a low angle thrust fault [*Ekstrom et al.*, 1992] (Figure 14b), to be compared with Figures 7 and 13. The observed aftershock activity is indicated in Figure 14b, although there is no evidence on whether dynamic branching occurred in this case (the fault geometry is from seismic reflection profiling [*Meltzer*, 1989]). Nucleation on a shallow dip, like for the 12°−14° of the 1985 Kettleman Hills event, corresponds to low inclination of S_{max} with the slightly curved main fault, $\Psi = 12°−14°$, and a branching angle (if the compressional branch was activated) $\varphi = +15°$ on the compressional side. Branching to the compressional side is indeed favored for such prestress state (see our simulations, Figures 7 and 13). This was an unusually slow earthquake [*Ekstrom et al.*,

1992], so the field data in Figure 14b should best be compared with Figure 13 looking at the second row for the proper branching angle, and the left side panel for the lowest rupture velocity that we have considered in the simulations. If our simulations reflect real rupture behavior, the comparison suggests the plausibility that rupture followed the branched fault structures shown in Figure 14b, with no continuation on the main fault after branching.

[53] As a strike-slip example, for the 1992 Landers rupture [*Sowers et al.*, 1994] (Figure 14c), S_{max} is taken from stress orientations in the Landers region determined by *Hardebeck and Hauksson* [2001] to be at approximately $\Psi = 60°$ with the trace of the Johnson Valley fault where it branched to the extensional side onto the Kickapoo fault, with the angle $\varphi = 30°$. The rupture also continued a few kilometers on the main (Johnson Valley) fault. This too is consistent with our results for the high inclination of S_{max} cases, $\Psi = 56°$, (Figure 10), last row. Our simulations suggest that in this case there should be branching, but that rupture continuation along the main fault should also occur, as is observed. The rupture, however, died out on the Johnson Valley Fault a short distance after branching and that remains unexplained in our simple modeling. A perspective is provided by *King et al.* [1994], who calculated Coulomb stress changes on optimally oriented faults due to the most recent four earthquakes with $M > 5$ in the region prior to the Landers event. While their Coulomb stress change is positive everywhere in the vicinity of the Johnson Valley to Kickapoo branch, and also along most of the region which ruptured in the Landers event, when one continues NW along the Johnson Valley Fault a region is encountered for which their stress change is instead negative. The dynamic rupture arrested shortly after propagating into that region of negative stress change (a similar result applies to where the rupture arrested to the SE along the Homestead Valley Fault). The negative stress changes are modest, of the order of 0.1 MPa, but may be related to why the rupture arrested.

[54] A second strike-slip example is the Imperial Valley 1979 earthquake [*Archuleta*, 1984] (Figure 14d). The approximate S_{max} direction is poorly constrained but may be estimated to be approximately north-south, based on stress directions reported by *Hardebeck and Hauksson* [1999] along a profile somewhat to the northwest near the Salton Sea. That leads to $\Psi \approx 37°$ with the main fault, where it branched, on the extensional side, at approximately $\varphi = -34°$ onto the Brawley fault. This is the least definitive case because of uncertainty of the prestress direction, but seems again interpretable with the results shown in Figure 11, last row. Again, our simulations show that progression of rupture on both the main fault as well as the branch would be encouraged.

[55] The continental field cases discussed above are the same set considered in *Poliakov et al.* [2002], but with new insights added on the basis of our present numerical simulations of branched rupture. Recently, there has been reported [*Park et al.*, 2002] yet another thrust example with branching, at the larger scale of a convergent plate boundary interface (Figure 14e). That is in the form of splay faulting from the great thrust interface of the Nankai Trough subduction zone. *Park et al.* [2002] used multichannel seismic reflection along three profiles perpendicular to the trough
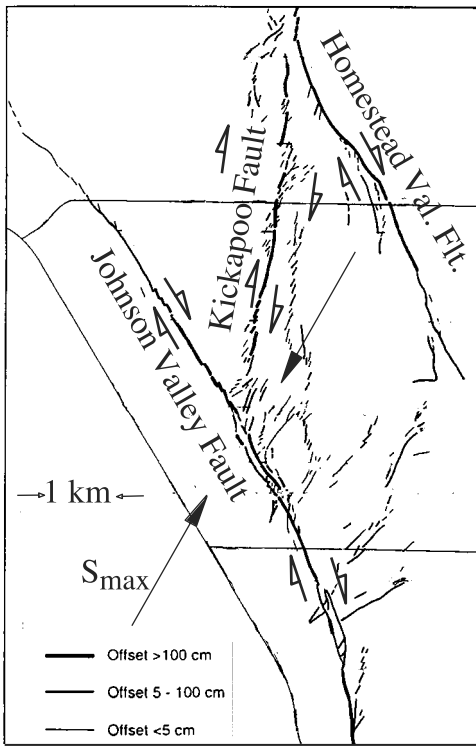
San Fernando 1971
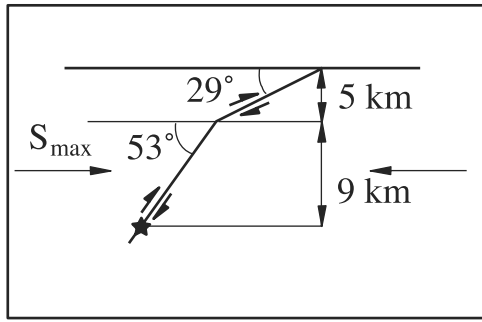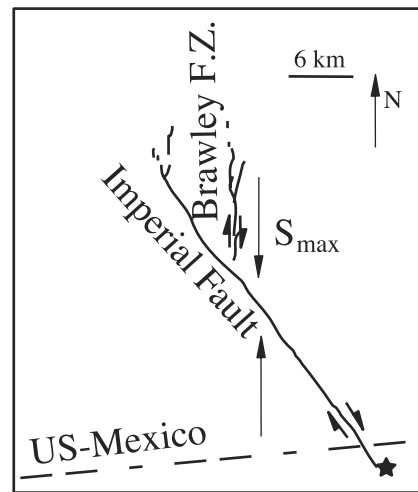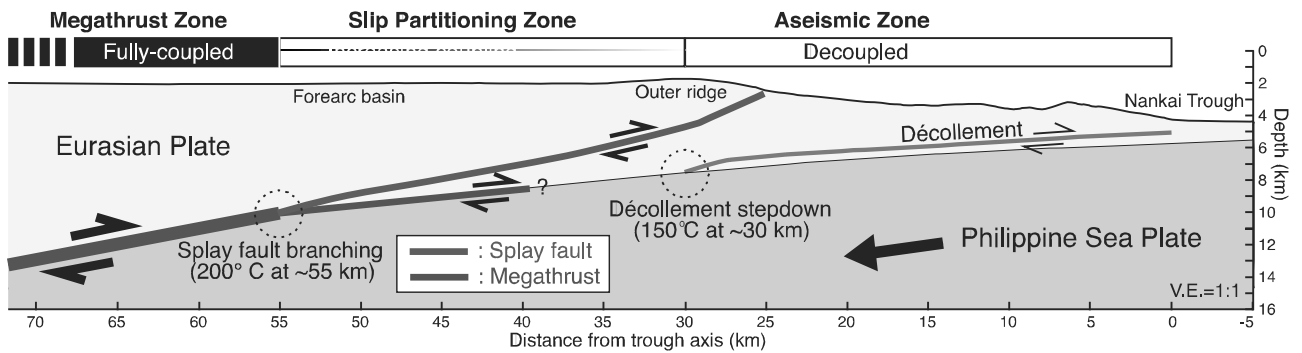

(a)

Kettleman Hills 1985
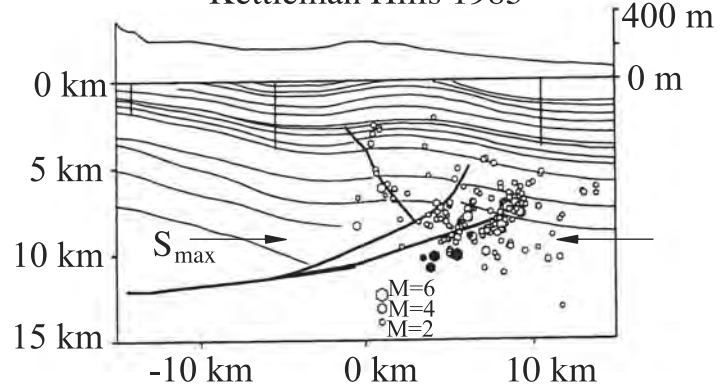
(b)

Landers 1992

(c)

Imperial Valley 1979

(d)

(e)

[see also *Nakanishi et al.*, 2002], in the vicinity of the *M* = 8.1 Tonankai 1944 event, to identify a splay fault structure which branches upward into the sedimentary wedge from the interface between subducted ocean floor and the wedge at around 10 km depth. The splay begins at around 50−55 km landward from the trough axis and, being seen on all three profiles, is assumed to extend at least the 100 km along strike between the outer two profiles. Also, because penetration of the splay fault with the ocean floor is associated with a local bathymetric gradient, *Park et al.* [2002] conjecture that the splay moved seismically during the event. The main fault, downdip from the splay junction, is inferred from the reflection data to be precisely at the interface between the sedimentary wedge and subducted seafloor.

[56] We measured angles from the three poststack depth−migrated profiles shown in Figure 2 of *Park et al.* [2002] to determine that the branching angle of the splay had the range φ = +3° to +10°, depending on profile, with average of 6°. Assuming that the principal precompression is horizontal, we can equate Ψ to the slope of the plate interface at the junction where the splay branches off into the sedimentary wedge. That gives Ψ = 7° to 8°, again depending on profile, with an average of 8°. Thus this case is closest to Figure 13, second row of panels, although both the φ and Ψ are somewhat smaller than in the simulations shown there. The results suggest that seismic rupture would surely follow the branch in that case, supporting the conjecture of *Park et al.* [2002] that the splay was active coseismically. Also, because of stress shadowing effects, which would be even stronger here than in the simulations because of the lower φ, we would predict that negligible seismic slip continued along the plate interface (main fault surface) updip of the splay junction. While branching examples in thrust earthquakes may be successfully interpreted from our results for a homogeneous medium, in reality there remains the possibility that bending of rupture is significantly affected by the existence of material boundaries, such as for a sedimentary region above ocean crust.

6. Conclusion

[57] We simulated rupture along dynamically self-chosen paths in branched fault systems, clarifying the effects of prestress state, rupture velocity and branch angle on dynamic branching.

[58] First, we found that the prestress state has a significant effect on the most favored direction for dynamic branching, which switches from the extensional to the compressive side as we consider progressively shallower angles of the direction of maximum precompression with the fault plane. That effect was predicted qualitatively in the analysis of branching conditions by *Poliakov et al* [2002]. It is also consistent with the comparison by *Aochi and Fukuyama* [2002] of simulation results, for rupture through the Johnson Valley to Kickapoo junction in the Landers 1992 event, based on different assumptions on the prestress orientation; the Kickapoo branch was chosen only for the steeper of their two stress orientations.

[59] Second, as suggested by *Kame and Yamashita* [1999a, 1999b] and *Poliakov et al.* [2002], we found that the enhanced dynamic stressing of a rapidly propagating rupture could nucleate failure on a fault which would not necessarily be judged the most favorably oriented one based on the prestress state. That effect is most pronounced as rupture velocity approaches the limiting velocity c_R, the Rayleigh wave velocity for mode II. It occasionally enables simultaneous rupture on both the main and a branch fault.

[60] Third, we clarified the effect of the branching angle. Simultaneous rupture propagation on both faults after bifurcation will be more difficult for smaller branching angle due to stress interaction that suppresses rupture on the other fault through stress shadowing.

[61] Despite the fact that the directions of principal stresses are often poorly known, we could compare our results with some better constrained field examples, discussed by *Poliakov et al.* [2002]. We found that the observed or inferred rupture paths in those field examples were consistent with the results of our simulations, when done for comparable prestress directions, branching angles and, in the cases for which there was information on it, rupture velocity.

[62] Using the boundary integral equation method or certain other modern computational methodologies, we are approaching a stage at which we can deterministically predict the rupture path of a forthcoming earthquake on an actual complex fault system with branches, at least assuming that its geometry is known. However, the results will depend on constitutive and loading parameters. Our studies suggest that, among other parameters, it will be important to know the prestress state along the fault system and, particularly, principal directions near any branching junctions. These stress directions should include not just the regional tectonic stress field but also the effects from previous earthquakes on the fault system, which may cause strong local deviations from the larger-scale stress field. Further, the path chosen at such junctions will depend also on rupture speed as they are approached, and that is not easily predicted. Nevertheless, it is important to advance such studies for their contribution to seismic risk estimates. Other questions to be addressed are the repeatability of nucleation sites of the largest earthquakes and of the directivity of rupture propagation in such complex fault systems.

Figure 14. (opposite) Field examples of earthquake ruptures exhibiting off-main-fault branching; parts (a), (b) and (d) from Figure 16 of *Poliakov et al.* [2002]. (a) San Fernando 1971 earthquake, based on *Heaton and Helmberger* [1979]. (b) Kettleman Hills 1985 earthquake, adapting diagram with fault and earthquake locations from *Ekstrom et al.* [1992]. (c) Johnson Valley 1992 rupture, at start of the Landers earthquake, branching onto the Kickapoo fault zone; fault map, with fault slip scaling with line thickness (thickest >100 cm), from *Sowers et al.* [1994]; other lines are roadways. (d) Imperial Valley 1979 rupture branching onto the Brawley fault zone, redrawn based on *Archuleta* [1984]. (e) Schematic cross section of the updip portion of the Nankai subduction zone, from Figure 3 of *Park et al.* [2002] (reprinted with permission; copyright 2002 American Association for the Advancement of Science).

[63] Our present analysis is two-dimensional, a case for which adequate grid resolution can be achieved within present computer limits to definitively resolve features of the slip-weakening process at branch junctions. Nevertheless, 2-D models are necessarily only an approximation. At least two 3-D features, present in the modeling by *Aochi and Fukuyama* [2002], must play a role in fault branching. These are the depth distribution of rupture velocity (because of the presence of sediments as well as different groundwater conditions at shallow depths, v_r will generally be slower there), and the irregular shape of a rupture front, which would therefore not normally reach all locations along a branching intersection simultaneously like in the 2-D model. More 3-D modeling and careful analysis of field cases should show in the future how critical are such factors.

Appendix A: Solution for Static Preslip on a Nucleation Zone

[64] Applying a discretization where a constant tangential slip (D) is assumed within each spatial element (Δs) in the elastostatic BIE, we can write the incremental tangential traction due to static slip in the following symbolic notation [*Kame and Yamashita*, 1999b],

$$\Delta\tau^i = \sum_j K_{\text{static}}^{i:j} D^j, \qquad (A1)$$

where i and j represent the discretized position on the fault. The term on the right hand side $K_{\text{static}}^{i:j}$ is the static stress kernel that indicates the shear stress at element i due to unit slip at element j. Although the incremental normal traction $\Delta\sigma_n$ has a similar symbolic form, we do not use it when we consider a planar fault where $\Delta\sigma_n$ is zero; no normal traction change occurs on a planar fault due to tangential slip on it. We use equation (A1) below.

[65] Consider a case with the nucleation zone consisting of N elements. In order to determine N unknown preslips in a static equilibrium that satisfies the slip-weakening Coulomb friction law (equation (1)), we have to solve the coupled N equations in equation (A1),

$$\tau^i = \sum_{j=1}^{N} K_{static}^{i:j} D^j + \tau^0, (i = 1, 2, \ldots, N), \qquad (A2)$$

where each preslip must meet equation (1) that is represented as a function of slip as

$$\tau^i = f(D^i), (i = 1, 2, \ldots, N). \qquad (A3)$$

Here τ^i and τ^0 represent the total traction and traction for the prestress state respectively.

[66] We can rewrite the problem in a form that

$$F_i(\mathbf{D}) = \sum_{j=1}^{N} K_{static}^{i:j} D^j + \tau^0 - f(D^i), \qquad (i = 1, 2, \ldots, N), \qquad (A4)$$

where $\mathbf{D} = (D^1, D^2, \ldots, D^N)$. The solution of $F_i(\mathbf{D}) = 0$, ($i = 1, 2, \ldots, N$) is numerically determined by using the Newton-Raphson method. The solution is then determined as a function of τ^0 which, to determine critical nucleation conditions, can be adjusted to make the stress equal to the peak stress at the center of the first locked cells beyond the slipping zone.

Appendix B: Damping Factor for Numerical Stability

[67] We introduce a damping procedure to suppress short-wavelength oscillation that appears in slip velocity as time steps go by [*Yamashita and Fukuyama*, 1996; *Kame and Yamashita*, 1999b]. After we determine slip velocity V^i over ruptured region(s) at each time step, we transform it into damped one using

$$V_{\text{damp}}^i = V^i + \alpha\left(V_{\text{damp}}^{i-1} + V_{\text{damp}}^{i+1} - 2V_{\text{damp}}^i\right). \qquad (B1)$$

In this paper, we set α to be 0.5, the same value used in *Yamashita and Fukuyama* [1996]. When rupture propagates only on the main fault, we just take a region for i from the left end to the right end of rupture. The above simultaneous equations with respect to the unknowns V_{damp}^i can then be solved numerically by using matrix inversion. After rupture is nucleated also on the branching fault, we always take two types of regions for i: (1) From the left end to the right end of rupture on the main fault. (2) From the left end of rupture on the main to the right end on the branching fault via the intersection point. In this case, we will have two different damped slip velocities within an overlap region between the left end and the branch intersection on the main fault. We apply damped velocity in that region from the results for region 1 unless the number of elements in region 2 is greater than that in region 1, and from the results for region 2 if it has more elements.

References

Andrews, D. J., Rupture velocity of plane strain shear crack, *J. Geophys. Res.*, *81*, 5679–5687, 1976.

Aochi, H., and E. Fukuyama, Three-dimensional non-planar simulation of the 1992 Landers earthquake, *J. Geophys. Res.*, *107*(B2), 2035, doi:10.1029/2000JB000061, 2002.

Aochi, H., E. Fukuyama, and M. Matsu'ura, Spontaneous rupture propagation on a non-planar fault in 3D elastic medium, *Pure Appl. Geophys.*, *157*, 2003–2027, 2000a.

Aochi, H., E. Fukuyama, and M. Matsu'ura, Selectivity of spontaneous rupture propagation on a branched fault, *Geophys. Res. Lett.*, *27*, 3635–3638, 2000b.

Aochi, H., R. Madariaga, and E. Fukuyama, Effect of normal stress during rupture propagation along nonplanar faults, *J. Geophys. Res.*, *107*(B2), 2038, doi:10.1029/2001JB000500, 2002.

Archuleta, R. J., A faulting model for the 1979 Imperial Valley earthquake, *J. Geophys. Res.*, *89*, 4559–4585, 1984.

Broberg, K. B., *Cracks and Fracture*, Academic, San Diego, Calif., 1999.

Cocco, M., and J. R. Rice, Pore pressure and poroelasticity effects in Coulomb stress analysis of earthquake interactions, *J. Geophys. Res.*, *107*(B2), 2030, doi:10.1029/2000JB000138, 2002.

Cochard, A., and R. Madariaga, Dynamic faulting under rate-dependent friction, *Pure Appl. Geophys.*, *142*, 419–445, 1994.

Ekstrom, G., R. S. Stein, J. P. Eaton, and D. Eberhart-Phillips, Seismicity and geometry of a 110 km-long blind thrust fault: 1. The 1985 Kettleman Hills, California, earthquake, *J. Geophys. Res.*, *97*, 4843–4864, 1992.

Freund, L. B., *Dynamic Fracture Mechanics*, Cambridge Univ. Press, New York, 1990.

Hardebeck, J. L., and E. Hauksson, Role of fluids in faulting inferred from stress field signatures, *Science*, *285*, 236–239, 1999.

Hardebeck, J. L., and E. Hauksson, Crustal stress field in southern California and its implications for fault mechanics, *J. Geophys. Res.*, *106*, 21,859–21,882, 2001.

Heaton, T. H., and D. V. Helmberger, Generalized ray models of the San-Fernando earthquake, *Bull. Seismol. Soc. Am.*, *69*, 1311–1341, 1979.

Ida, Y., Cohesive force across the tip of a longitudinal-shear crack and Griffith's specific surface energy, *J. Geophys. Res.*, *77*, 3796–3805, 1972.

Kame, N., and T. Yamashita, A new light on arresting mechanism of dynamic earthquake faulting, *Geophys. Res. Lett.*, *26*, 1997–2000, 1999a.

Kame, N., and T. Yamashita, Simulation of spontaneous growth of dynamic crack without constraints on the crack tip path, *Geopys. J. Int.*, *139*, 349–358, 1999b.

King, G. C. P., Speculations on the geometry of the initiation and termination process of earthquake rupture and its relation to morphology and geological structure, *Pure Appl. Geophys.*, *124*, 567–585, 1986.

King, G. C. P., and J. Nabelek, The role of fault bends in the initiation and termination of earthquake rupture, *Science*, *228*, 984–987, 1985.

King, G. C. P., R. S. Stein, and J. Lin, Static stress changes and the triggering of earthquakes, *Bull. Seismol. Soc. Am.*, *84*, 935–953, 1994.

Langston, C. A., The February 9, 1971 San Fernando earthquake: A study of source finiteness in teleseismic body waves, *Bull. Seismol. Soc. Am.*, *68*, 1–29, 1978.

Meltzer, A., Crustal structure and tectonic evolution: Central California, Ph.D. thesis, Rice Univ., Houston, Tex., 1989.

Nakanishi, A., N. Takahashi, J.-O. Park, S. Miura, S. Kodaira, Y. Kaneda, N. Hirata, T. Iwasaki, and M. Nakamura, Crustal structure across the coseismic rupture zone of the 1944 Tonankai earthquake, the central Nankai Trough seismogenic zone, *J. Geophys. Res.*, *107*(B1), 2007, doi:10.1029/2001JB000424, 2002.

Palmer, A. C., and J. R. Rice, The growth of slip surfaces in the progressive failure of over-consolidated clay, *Proc. R. Soc. London, Ser. A*, *332*, 527–548, 1973.

Park, J.-O., T. Tsuru, S. Kodaira, P. R. Cummins, and Y. Kaneda, Splay fault branching along the Nankai subduction zone, *Science*, *297*, 1157–1160, 2002.

Poliakov, A. N. B., R. Dmowska, and J. R. Rice, Dynamic shear rupture interactions with fault bends and off-axis secondary faulting, *J. Geophys. Res.*, *107*(B11), 2295, doi:10.1029/2001JB000572, 2002.

Rice, J. R., The mechanics of earthquake rupture, in *Physics of the Earth's Interior*, edited by A. M. Dziewonski and E. Boschi, *Proc. Int. Sch. Phys. "Enrico Fermi"*, *78*, 555–649, 1979.

Sibson, R. H., Stopping of earthquake ruptures at dilatational fault jogs, *Nature*, *316*, 248–251, 1985.

Sowers, J. M., J. R. Unruh, W. R. Lettis, and T. D. Rubin, Relationship of the Kickapoo fault to the Johnson Valley and Homestead Valley faults, San Bernardino County, California, *Bull. Seismol. Soc. Am.*, *84*, 528–536, 1994.

Yamashita, T., and E. Fukuyama, Apparent critical slip displacement caused by the existence of a fault zone, *Geopys. J. Int.*, *125*, 459–472, 1996.

Yamashita, T., and Y. Umeda, Earthquake rupture complexity due to dynamic nucleation and interaction of subsidiary faults, *Pure Appl. Geophys.*, *143*, 89–116, 1994.

———————————

R. Dmowska and J. R. Rice, Department of Earth and Planetary Sciences and Division of Engineering and Applied Sciences, Harvard University, Cambridge, MA 02138, USA. (dmowska@esag.harvard.edu; rice@esag.harvard.edu)

N. Kame, Department of Earth and Planetary Sciences, Faculty of Science, Kyushu University, 6-10-1 Hakozaki, Higashi-ku, Fukuoka 812-8581, Japan. (kame@geo.kyushu-u.ac.jp)